OCT 25 2001

0830-L-02 NAS 1-29/3-2: 01-10

NASA TechBriefs

National Aeronautics and
Space Administration

Electronic Components and Circuits

(384)

Electronic Systems

Physical Sciences

Materials

Computer Programs

Mechanics

Machinery

Fabrication Technology

Mathematics and Information Sciences

Life Sciences

Am 2002 064147 C

INTRODUCTION

Tech Briefs are short announcements of innovations originating from research and development activities of the National Aeronautics and Space Administration. They emphasize information considered likely to be transferable across industrial, regional, or disciplinary lines and are issued to encourage commercial application.

Availability of NASA Tech Briefs and TSPs

Requests for individual Tech Briefs or for Technical Support Packages (TSPs) announced herein should be addressed to

National Technology Transfer Center
Telephone No. **(800) 678-6882** or via World Wide Web at **www2.nttc.edu/leads/**

Please reference the control numbers appearing at the end of each Tech Brief. Information on NASA's Commercial Technology Team, its documents, and services is also available at the same facility or on the World Wide Web at **www.nctn.hq.nasa.gov**.

Commercial Technology Offices and Patent Counsels are located at NASA field centers to provide technology-transfer access to industrial users. Inquiries can be made by contacting NASA field centers and program offices listed below.

NASA Field Centers and Program Offices

Ames Research Center
Carolina Blake
(650) 604-1754 or
cblake@mail.arc.nasa.gov

Dryden Flight Research Center
Jenny Baer-Riedhart
(661) 276-3689 or
jenny.baer-riedhart@dfrc.nasa.gov

Goddard Space Flight Center
George Alcorn
(301) 286-5810 or
galcorn@gsfc.nasa.gov

Jet Propulsion Laboratory
Merle McKenzie
(818) 354-2577 or
merle.mckenzie@jpl.nasa.gov

Johnson Space Center
Hank Davis
(281) 483-0474 or
henry.l.davis1@jsc.nasa.gov

John F. Kennedy Space Center
Jim Aliberti
(321) 867-6224 or
Jim.Aliberti-1@ksc.nasa.gov

Langley Research Center
Sam Morello
(757) 864-6005 or
s.a.morello@larc.nasa.gov

Glenn Research Center
Larry Viterna
(216) 433-3484 or
cto@grc.nasa.gov

George C. Marshall Space Flight Center
Vernotto C. McMillan
(256) 544-2615 or
vernotto.mcmillan@msfc.nasa.gov

John C. Stennis Space Center
Kirk Sharp
(228) 688-1929 or
technology@ssc.nasa.gov

NASA Program Offices
At NASA Headquarters there are seven major program offices that develop and oversee technology projects of potential interest to industry:

Carl Ray
Small Business Innovation Research Program (SBIR) & Small Business Technology Transfer Program (STTR)
(202) 358-4652 or
cray@mail.hq.nasa.gov

Dr. Robert Norwood
Office of Commercial Technology (Code RW)
(202) 358-2320 or
rnorwood@mail.hq.nasa.gov

John Mankins
Office of Space Flight (Code MP)
(202) 358-4659 or
jmankins@mail.hq.nasa.gov

Terry Hertz
Office of Aero-Space Technology (Code RS)
(202) 358-4636 or
thertz@mail.hq.nasa.gov

Glen Mucklow
Office of Space Sciences (Code SM)
(202) 358-2235 or
gmucklow@mail.hq.nasa.gov

Roger Crouch
Office of Microgravity Science Applications (Code U)
(202) 358-0689 or
rcrouch@hq.nasa.gov

Granville Paules
Office of Mission to Planet Earth (Code Y)
(202) 358-0706 or
gpaules@mtpe.hq.nasa.gov

NASA TechBriefs

National Aeronautics and
Space Administration

October 2001
01-10

5 Electronic Components and Circuits

11 Physical Sciences

19 Materials

27 Computer Programs

33 Mechanics

39 Machinery

47 Fabrication Technology

51 Mathematics and Information Sciences

55 Life Sciences

This document was prepared under the sponsorship of the National Aeronautics and Space Administration. Neither the United States Government nor any person acting on behalf of the United States Government assumes any liability resulting from the use of the information contained in this document, or warrants that such use will be free from privately owned rights.

4

BLANK PAGE

Electronic Components and Circuits

Hardware, Techniques, and Processes

7 Ultra-Efficient K_a-Band MMIC Power Amplifier

8 Implementing Permutation Matrices by Use of Quantum Dots

BLANK PAGE

Ultra-Efficient K_a-Band MMIC Power Amplifier

The design is a substantial advance in the state of the art.

Lyndon B. Johnson Space Center, Houston, Texas

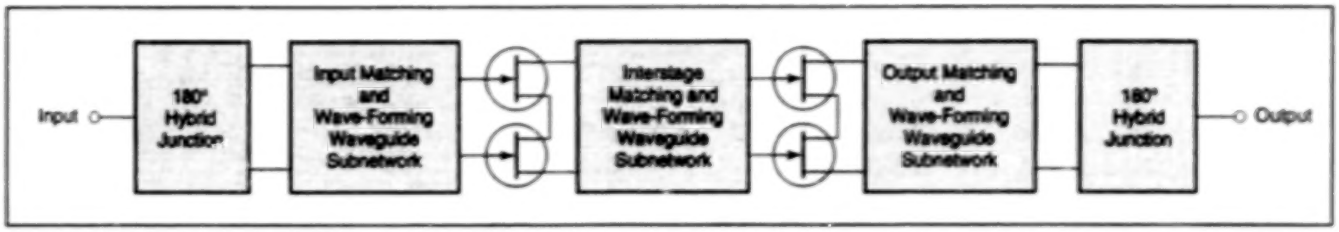

Figure 1. **High-Performance PHEMTs** would be connected in an impedance-matching, wave-forming network to obtain high power efficiency.

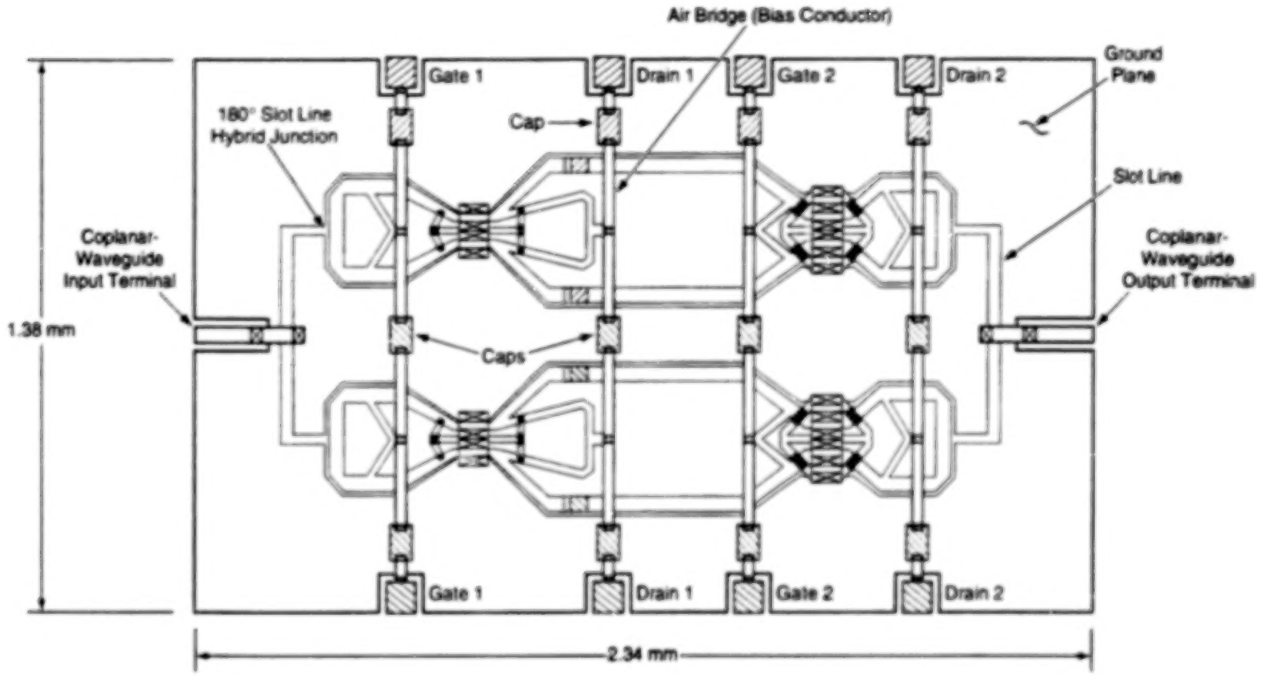

Figure 2. The **Ultra-Efficient MMIC Power Amplifier** would contain two mirror-image, two-stage amplifiers connected in parallel to double the output power. The layout would be essentially planar, with no via holes (which would contribute parasitic inductances).

A proposed monolithic microwave integrated circuit (MMIC) power amplifier has been designed to operate at frequencies around 28 GHz. According to a computer simulation of performance, this amplifier would operate at a power-added efficiency of more than 60 percent, which is more than 20 percent above that of the prior state-of-the-art power amplifiers in this frequency range.

The design calls for a two-stage amplifier (see Figure 1), each stage containing a pair of pseudomorphic high-electron-mobility transistors (PHEMTs) in a push/pull configuration. The PHEMTs would be biased for class-B or -C operation (conduction angle ≤180° at the fundamental frequency). The push/pull configuration would be achieved by connecting the PHEMTs to each other and to the input and output terminals by embedding them in a coplanar waveguide network of microstrip conductor lines and slots (see Figure 2). The network would include input and output balun transformers in the form of slot/line hybrid junctions.

Efficiency greater than the theoretical maximum of $\pi/4$ for classical class-B operation would be achieved by a wave-forming design concept directed toward minimizing the time integral of (drain voltage × drain current) for a given output level at the fundamental frequency. This concept involves (1) exploiting the specific transfer characteristics of the high-performance PHEMTs, to obtain approximately square-wave drain-voltage waveforms, and (2) suppressing the harmonic contents of the square waves on the way to the output terminal to shape the final output waveform into a fundamental-frequency sinusoid. For this purpose, the waveguide network would include wave-forming subnetworks in which the harmonics would be terminated in reactive impedances.

This work was done by James M. Schellenberg of Schellenberg Associates for **Johnson Space Center**. *Further information is contained in a TSP [see page 1].*

MSC-22503

Implementing Permutation Matrices by Use of Quantum Dots

Computing circuits could be simplified in that signal paths could be crossed.

NASA's Jet Propulsion Laboratory, Pasadena, California

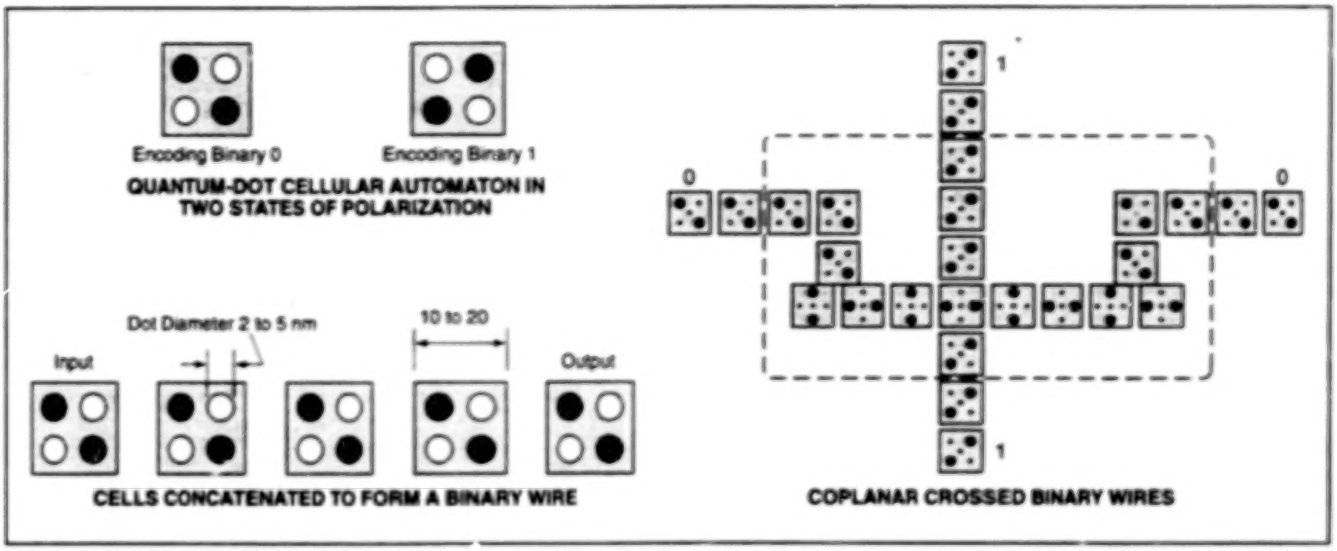

Figure 1. **Quantum-Dot Cellular Automata** can be assembled into binary wires, which can cross without adverse effect.

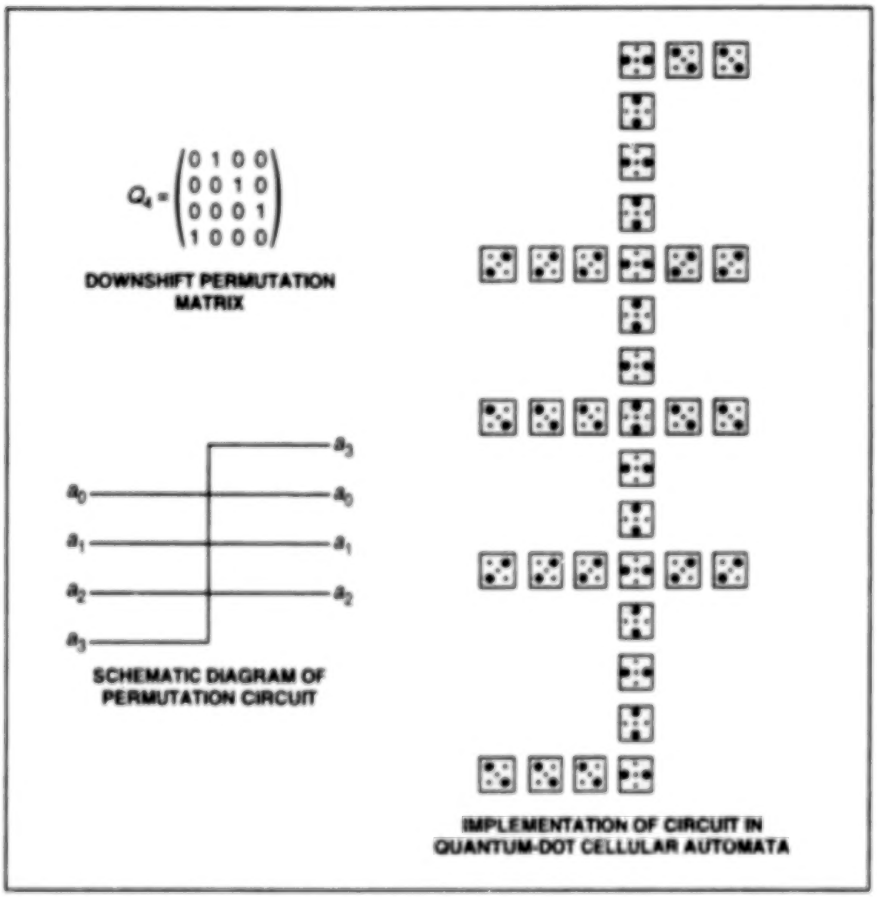
$Q_4 = \begin{pmatrix} 0 & 1 & 0 & 0 \\ 0 & 0 & 1 & 0 \\ 0 & 0 & 0 & 1 \\ 1 & 0 & 0 & 0 \end{pmatrix}$
DOWNSHIFT PERMUTATION MATRIX
a_0
a_1
a_2
a_3
a_3
a_0
a_1
a_2
SCHEMATIC DIAGRAM OF PERMUTATION CIRCUIT
IMPLEMENTATION OF CIRCUIT IN QUANTUM-DOT CELLULAR AUTOMATA

Figure 2. **A Simple QCA Circuit** would implement the downshift permutation matrix Q_4.

Integrated circuits of a proposed type based on quantum-dot cellular automata (QCA) would implement permutation matrices. These circuits would serve as prototype building blocks for demonstrating the feasibility of quantum-dot-based computing and for the further development of increasingly complex and increasingly capable quantum-dot-based computing circuits. Permutation matrices were chosen as part of the basis of this development because (1) they play a major role in fast transforms (e.g., the fast Fourier, cosine, and Hartley transforms) that arise in the processing of signals and images and that are amenable to parallel computing by application-specific integrated circuits and (2) in principle, they could be implemented directly in the patterns of circuits of the proposed type.

As the development of very-large-scale integrated (VLSI) circuitry approaches the lower limits of practical feature sizes, QCA may offer an alternative that will enable further miniaturization. Of equal if not greater significance is the expectation that QCA may enable a great simplification of VLSI circuit patterns while affording capabilities that, heretofore, have not existed.

At present, wherever two wires in a VLSI circuit cross each other, the wires must not be in the same plane; that is, there must be a layer of electrical insulation between them (unless, of course, they are meant to be connected at the intersection). Much of the complexity and hence cost of VLSI design is associated with minimization of data routing and assignment of layers to minimize crossing of wires. The proposed circuits would enable one to take advantage of a unique feature of QCA; namely, the possibility of coplanar crossing of signal paths. This feature is what makes it possible, in principle, to implement various permutation matrices directly in coplanar patterns of quantum-dot circuit elements. Such a direct and compact implementa-

tion would be extremely costly if not impossible in conventional complementary metal oxide/semiconductor (CMOS) VLSI integrated circuitry.

A quantum-dot cellular automaton contains four quantum dots positioned at the corners of a square (see Figure 1). The cell contains two extra mobile electrons that can tunnel (in the quantum-mechanical sense) between neighboring dots. Tunneling out of the cell is assumed to be completely suppressed by the potential barriers between neighboring cells. The Coulomb repulsion between the two electrons tends to make them occupy antipodal dots in the cell. For an isolated cell, there are two energetically equivalent arrangements (denoted polarization states) of the extra electrons. The cell polarization is used to encode binary information.

The polarization of a nonisolated cell depends on interactions with neighboring cells. The interaction between cells is one of Coulomb repulsion only (no current flows between cells) and provides the basis for computing with QCA. Theoretically, universal logic gates and binary wires could be constructed by assembling QCA of suitable design in suitable patterns. As to the possibility of coplanar crossing of signal paths without adverse effect, a compete theoretical explanation would exceed the space available for this article, but one can gain a partial, qualitative understanding from the illustration of crossed binary QCA wires in the bottom part of Figure 1.

One of the fundamental permutation matrices is the downshift permutation matrix, which is given by

$$Q_n(i,j) = \begin{cases} 1 & \text{if } j = i+1 \pmod{n} \\ 0 & \text{otherwise} \end{cases}$$

where n is the number of elements to be permuted. Figure 2 illustrates a proposed QCA circuit that would implement the permutation matrix Q_4.

This work was done by Amir Fijany, Nikzad Toomarian, and Matthew Spotnitz of Caltech for **NASA's Jet Propulsion Laboratory**. *Further information is contained in a TSP [see page 1].*
NPO-20801

BLANK PAGE

Physical Sciences

Hardware, Techniques, and Processes

13 Improved Automated System for Transferring Liquid Helium
13 Multibeam Beacon Laser Assembly
14 Vibrational and Thermal Isolator for Spacecraft Electronics
15 Commercial-Tolerance Superachromatic Near-IR Lens System
16 Algorithm for Computing Dynamics of Molecules
16 Improving Thin Foil X-Ray Mirrors
17 Improved Fiber-Pigtailed Non-Planar Ring Oscillator Laser

Books and Reports

17 First-Generation Integrated Free-Flying Micro-Spacecraft
18 DNS of a Transitional Supercritical C_7H_{16}/N_2 Mixing Layer

BLANK PAGE

Improved Automated System for Transferring Liquid Helium

Consumption of liquid helium would be reduced by optimizing use of vapor for precooling.

Goddard Space Flight Center, Greenbelt, Maryland

An improved automated system for transferring liquid helium from a supply tank to an end-use cryostat has been proposed. Like automated systems developed previously for the same purpose, this system would reduce the time that must be spent by technicians in replenishing cryostats in equipment required to operate for times longer than cryostat holding times. However, relative to prior automated liquid-helium-transfer systems, this system would operate in a more nearly optimum manner so as to reduce the consumption of liquid helium. Examples of equipment with which this system could be used include apparatuses for long-duration scientific experiments and large cooled electromagnets in medical imaging systems.

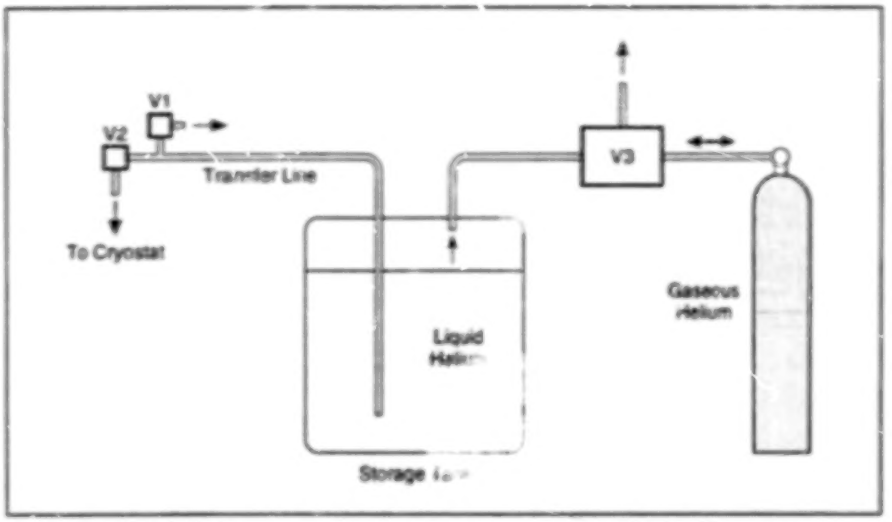

Three Valves Would Control the Flows of liquid and gaseous helium in this system.

The system would control the flow of liquid helium through a transfer line and would control ancillary flows of helium gas generated by vaporization of the liquid helium. It would precool the transfer line, as needed, to minimize boiling of liquid helium in the line and would prevent the flow of warm gas into the cryostat.

The system would include a liquid-level sensor in the cryostat, an electronic control circuit, three valves (V1, V2, and V3, as shown in the figure), and a temperature sensor in the transfer line upstream of V1. The transfer line would comprise a stainless steel inner tube for carrying liquid helium, surrounded by a vacuum jacket to minimize loss of heat, surrounded by an outer tube for the passage of helium gas to cool the parts within. V2 would control the flow of liquid helium through the inner tube. V1, located at the top of the inner tube, would control the flow of helium gas from the inner tube to the outer tube. After flowing though the outer tube, the helium gas could be vented, or, if necessary for safety, it could be collected. V3 would be used to stabilize the system by bleeding off helium gas generated by vaporization in the storage tank.

Upon sensing that the cryostat liquid level was below the minimum acceptable level, the system would trigger a regulator to pressurize the storage tank to pump liquid helium into the transfer line. Simultaneously, V1 would be opened. The initial warmth of the transfer line would cause some of the liquid helium to boil; the resulting vapor would flow through V1 into the outer tube. Once the temperature measured just upstream of V1 had fallen to predetermined level near the boiling temperature of helium, V1 would be closed and then V2 would be opened so that liquid helium could flow through the inner tube to the cryostat. When the cryostat liquid level reached the maximum acceptable level, the transfer would be considered to be complete and hence both V1 and V2 would be closed.

This work was done by G. Mark Cushman and Richard M. Gummer of **Goddard Space Flight Center**.

Inquiries concerning rights for the commercial use of this invention should be addressed to the Patent Counsel, Goddard Space Flight Center [see page 1]. Refer to GSC-14106.

Multibeam Beacon Laser Assembly

Scintillation is reduced, relative to a single-laser-beam beacon.

NASA's Jet Propulsion Laboratory, Pasadena, California

An optical assembly that combines the output of mutually incoherent lasers into a multibeam source for transmission into free-space was designed, assembled, and tested. This design was motivated by the need for ground-based beacon sources required for broadcasting laser beams to spaceborne, satellite-to-ground free-space optical communications systems. These beacons will provide a pointing and tracking reference for the spaceborne optical communications system and be used to uplink commands and data to the spacecraft. The assembly was field tested by broadcasting the beams through a 0.6-m-aperture telescope over a mountaintop-to-mountaintop 45-km atmospheric path, with receiving sensors located at the other end. The key advantages of the design are the following:

- Reduction in atmospheric-turbulence-induced irradiance fluctuations, due to incoherent averaging of the overlapping beams in the far-field, effectively eliminating or greatly reducing fades experienced by the spaceborne sensor.
- The distribution of the required optical power among multiple beams, which in some cases allows greater optical throughput without exceeding the damage threshold of optical surfaces and in other cases can help maintain eye-safe irradiance levels at the transmitting aperture.

The assembly (see figure) includes four multimode fiber-coupled (62.5-μm

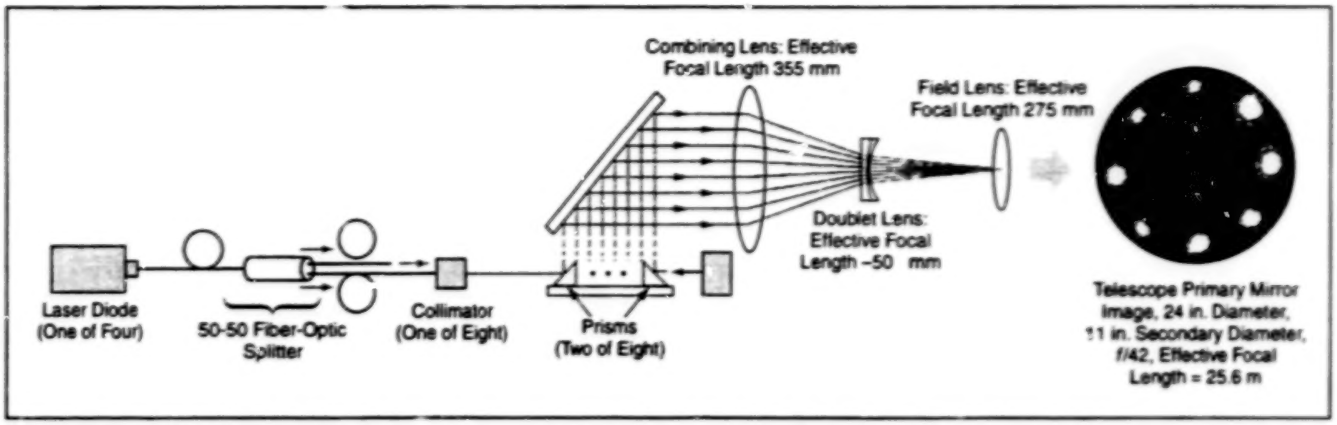
Combining Lens: Effective Focal Length 355 mm
Field Lens: Effective Focal Length 275 mm
Doublet Lens: Effective Focal Length –50 mm
Laser Diode (One of Four)
50-50 Fiber-Optic Splitter
Collimator (One of Eight)
Prisms (Two of Eight)
Telescope Primary Mirror Image, 24 in. Diameter, 11 in. Secondary Diameter, f/42, Effective Focal Length = 25.6 m

The schematic shows how Eight Laser Beams are copropagated through a single telescope aperture. The inset shows a photograph of the individual laser spots on the telescope primary mirror. The beams overlap in the far-field and noncoherent averaging causes the atmosphere induced intensity fluctuations (scintillation) to be eliminated or greatly reduced.

core) laser diodes emitting at ~780 nm. The output of each laser is further split into two beams, using multimode fiber-optic splitters. The resulting outputs are each free-space coupled through 11-mm focal length collimators, resulting in an optical power of ~10 mW per beam. The collimated outputs are then aimed radially toward eight right-angled prisms (see figure) arranged symmetrically about the optical axis of an optical train consisting of a positive combining lens, followed by a negative doublet lens, and finally a field lens at the Coudé focus of the telescope. The telescope focal length used was 25 m. The entire optical assembly was chosen to provide a 123 μrad full-width (100-percent energy) beam divergence that also corresponded to ~42 mm subaperture spots arranged symmetrically on the primary mirror of the transmitting telescope.

The inset accompanying figure shows beam spots on the primary mirror. The spot sizes varied between 33 and 48 mm, resulting in a range of beam divergences.

In field tests, the expected reduction in atmospheric-turbulence-induced irradiance fluctuations was ascertained by measuring the normalized variance of the received power. Thus, an observed normalized variance range (also called scintillation index) of 0.8 to 1.3 observed for single beams was reduced to 0.13 to 0.55 upon combining all eight beams. The range of observed normalized variances were recorded over three separate campaigns conducted between June and September of 2000. The observed range of values is attributed to the variations in (1) the extent of beam overlap achieved and (2) variations in atmospheric turbulence over the period of measurements.

This work was done by Malcolm Wright, Abhijit Biswas, Norman Page, and Babak Sanii of Caltech for ***NASA's Jet Propulsion Laboratory****. Further information is contained in a TSP [see page 1].*

In accordance with Public Law 96-517, the contractor has elected to retain title to this invention. Inquiries concerning rights for its commercial use should be addressed to

Technology Reporting Office
JPL
Mail Stop 249-103
4800 Oak Grove Drive
Pasadena, CA 91109
(818) 354-2240

Refer to NPO-21119, volume and number of this NASA Tech Briefs issue, and the page number.

Vibrational and Thermal Isolator for Spacecraft Electronics

This is a relatively inexpensive, lightweight device for protecting low-power circuitry.

Lyndon B. Johnson Space Center, Houston, Texas

Engineers at Johnson Space Center have invented a relatively inexpensive, lightweight device that provides vibrational and thermal isolation for low-power electronic equipment. The device was developed for use in outer space, where it has already proven successful in connection with the Inter-Mars tissue-equivalent proportional counter on shuttle flights and in a gas proportional counter flown aboard the satellite of the TRW Small Spacecraft Technology Initiative. The device could also be used on Earth to isolate sensitive items from extremes of temperature and vibration.

Until now, vibration and thermal isolation have been provided, in general, by means specific to each electronic component, electronic circuit, or other item for which the need has occurred. Vibration isolation has been effected by use of little more than adjustable spring devices. Moreover, it has been necessary to consider a vibrationally isolated item to be surrounded by a dynamic envelope in which it can move, making it difficult to insulate or thermally isolate the item from any structure in its vicinity. Worse, for purposes of spaceflight, the prior art does not necessarily provide thermal control, electrical isolation, or protection against electromagnetic interference.

The present device (see figure) does provide thermal control, electrical isolation, and protection against electromagnetic interference. An item to be isolated is placed inside a boxlike shroud, wherein it is floated on pads made of Nomex (or equivalent) aramid felt that have been bonded to inside surfaces of the shroud. The shroud is hard-mounted on a spacecraft structure through four attachment feet.

During the intense vibrations associated with the spacecraft launch, the felt pads provide dynamic damping of the vibrational loads, keeping these loads to a level at or below that allowed by the design of the item to be isolated. In outer space, the felt pads provide thermal isolation for experiments. Inasmuch as the shroud is unpressurized, the only means of transfer of heat to or from the item to be isolated are conduction through the felt pads and radiation between the item and the inner shroud surfaces. Radiative heat transfer is controlled via judicious selec-

tion of the thermo-optical properties of both the interior and exterior surfaces of the shroud so that the net thermal effect is to satisfy the thermal requirements for the item to be isolated. The operation of the device, with and without external multilayer insulation (MLI), has been demonstrated in tests and in flight. The need to add MLI is determined for each application.

This device contains no mechanisms and is very inexpensive, in comparison with prior devices developed for the same purpose. Unlike in similar products, the dynamic envelope of the item to be isolated is contained within the shroud. Its versatile design has been demonstrated during operations in a variety of thermal and vibrational environments. The combination of the shroud and felt provides electrical isolation in addition to vibrational and thermal isolation. The felt is easily tailored: the number, initial compression, and density of the pads can all be varied to obtain the desired thermal and vibrational response.

This work was done by Steven L. Rickman, John P. McManamen, Sharon K. Whitcomb, Christopher P. Hansen, William C. Schneider, and Gautam D. Badhwar of **Johnson Space Center** *and Robert P. Dunn of Lockheed Martin.*
MSC-22761

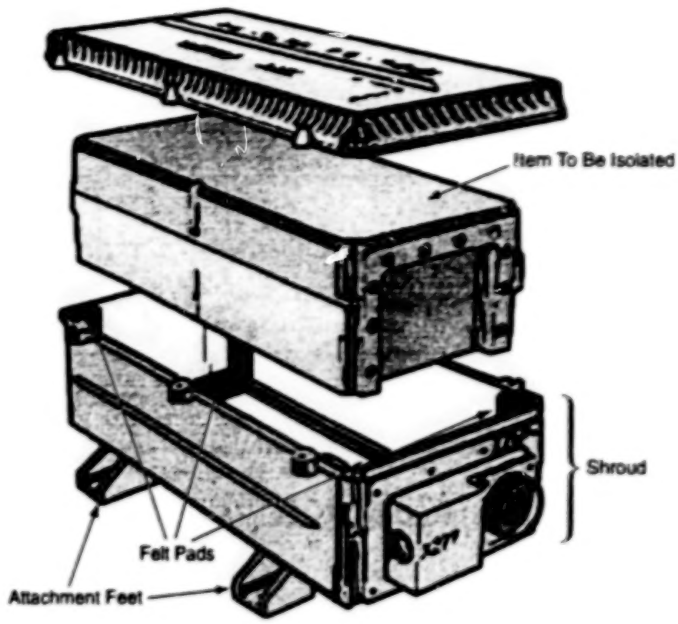

This **Device May Look Simple**, but the thermo-optical properties of the shroud surfaces and the mechanical and thermal properties of the felt pads are carefully engineered to satisfy specific requirements for thermal and vibrational isolation of the item to be placed inside.

Commercial-Tolerance Superachromatic Near-IR Lens System

Diffraction-limited performance is obtained even when tolerances are relaxed somewhat.

NASA's Jet Propulsion Laboratory, Pasadena, California

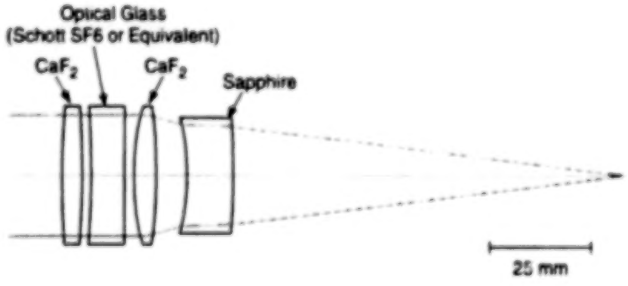

Lens Surface (Numbered From Left to Right)	Radius of Curvature, Millimeters	Axial Distance to Next Lens Surface, Proceeding Left to Right, Millimeters
1	220.44983	5.000000
2	-164.38136	2.000000
3	-202.29996	9.008424
4	-1017.12545	2.000000
5	51.05997	5.869715
6	-78.67031	7.557411
7	-61.82362	11.000000
8	-167.37928	

This **Four-Element Lens** gives diffraction-limited performance at wavelengths from 0.8 to 1.7 μm.

The figure depicts the optical layout and meridional-plane ray-trace diagram of a four-element superachromatic near-infrared (IR) lens system. The system features a 30-mm-diameter entrance pupil, a focal-length-to-diameter ratio (f/ number) of 4, and a field of view with a half-cone-angle width of 0.25°.

This optical design incorporates three key features:

1. Spectral bandwidth greater than one octave in the near IR.
2. Exceptionally low design geometric and chromatic aberrations. [Design root-mean-square (rms) geometric spot diameter <1 μm.]
3. Commercial-level optomechanical tolerances for diffraction-limited performance.

This system was designed to replace a prior lens system that could not satisfy the applicable performance requirements because its tolerances were too tight. This system offers diffraction-limited performance over the wavelength band from 0.8 to 1.7 μm, even when the component lenses are fabricated and assembled with commercial-level optomechanical tolerances.

This work was done by Hiroshi Kadogawa of Caltech for **NASA's Jet Propulsion Laboratory**. *Further information is contained in a TSP [see page 1].*
NPO-21078

Algorithm for Computing Dynamics of Molecules

Equations of motion are solved more efficiently.

NASA's Jet Propulsion Laboratory, Pasadena, California

The Newton-Euler Inverse Mass Operator (NEIMO) algorithm and software that implements the algorithm have been developed to reduce the amount of time needed to perform computational simulations of the dynamics of macromolecules. The NEIMO algorithm and the associated software are intended, in particular, for simulations of molecular motions at a space-time mesoscale, defined here as a length scale ranging from nanometers to micrometers and a time scale ranging from microseconds to milliseconds. Older molecular-dynamics algorithms and computer programs are not suitable for mesoscale simulations because they were formulated for the time scales, of the order of a microsecond or less, characteristic of such high-frequency degrees of freedom as stretching of molecular bonds.

If, in a macromolecular-dynamics computation, one constrains the high-frequency degrees of freedom and uses internal coordinates, one not only reduces the number of degrees of freedom but also enables the use of a larger time step in numerical integration. Doing so also eliminates friction in the simulated system, enabling fast and efficient searches among conformations. On the other hand, the use of internal coordinates leads to coupled equations of motion. The solution of the equations involves inversion of a dense mass matrix. Older algorithms that solve coupled equations of motion exhibit computational complexity proportional to $O(N^3)$, where $O(X)$ signifies a number of the order of X and N is the number of degrees of freedom in a simulated system. For example, for a rhinovirus containing nearly 500,000 atoms, it would be necessary to invert a 167,000-by-167,000 matrix at every time step — clearly impractical.

The NEIMO algorithm was derived within the theoretical framework of the spatial-operator formulation of multibody dynamics. This formulation, which has been discussed in a number of previous issues of *NASA Tech Briefs*, was conceived for modeling the dynamics of complex, articulated collections of bodies (principally, multiple-link robot arms); since its conception, this formulation has also been found to be useful for simulating the dynamics of a variety of complex systems, including molecules. The software that implements the NEIMO algorithm is a modified version of the DARTS computer program, which was also based on the spatial-operator formulation and was reported in "Program for Simulating Dynamics of Multibody Systems" (NPO-20168), *NASA Tech Briefs*, Vol. 22, No. 2 (February 1998), page 70.

The great advantage of NEIMO is that in comparison with the older algorithms, it involves much less computation. The computational complexity of the NEIMO algorithm is proportional to $O(N)$ — much less than $O(N^3)$ for multiple degrees of freedom. The NEIMO algorithm solves the constrained equations of motion efficiently by keeping all high-frequency modes fixed and reduces the number of degrees of freedom from $3M$ (where M is the number of atoms) to M. The remaining degrees of freedom are the dihedral ones.

This work was done by Abhinandan Jain, Guillermo Rodriguez, and Nagaranjan Vaidehi of Caltech for **NASA's Jet Propulsion Laboratory**. *Further information is contained in a TSP [see page 1].*

This software is available for commercial licensing. Please contact Don Hart of the California Institute of Technology at (818) 393-3425. Refer to NPO-20796.

Improving Thin Foil X-Ray Mirrors

Resolution and diameter would be increased.

Goddard Space Flight Center, Greenbelt, Maryland

A proposal has been made to develop improved thin foil, replicated conical mirrors for use in x-ray astrophysics. In the NASA astrophysical programs in which such mirrors are used, they are required to be lightweight, and to offer moderate angular resolution and high throughput to afford required sensitivity in the photon-energy band from 0.1 to 20 keV. In the proposed improvement program, emphasis would be placed on increasing resolution and diameter:

- Angular resolution would be increased from the current level (half-power diameter of 1 arc minute, achieved for the Astro-E mission) to a higher level (half-power diameter of 15 arc seconds, required for the Constellation-X mission).
- Mirrors with diameters as large as 1.6 m would be developed.

Increased angular resolution of replicated conical foil mirrors depends mostly on the geometric accuracy and microscopic roughness of the surface being replicated, and on the accuracy with which the foil reflectors are held in position in mirror structures. According to the proposal, precise conical mandrels with root-mean-square surface roughness less than 5 Å would be either fabricated in house or bought to demonstrate the ability to make precise reflectors. Polished quartz or Zerodur (or equivalent low-thermal-expansion glass) mandrels as well as less expensive diamond-turned nickel mandrels would be tested. The following three approaches would be investigated as means for increasing the accuracy of holding fixtures: (1) highly precise electrical-discharge machining, (2) diamond turning, and (3) application, to silicon fixtures, of microlithographic and etching techniques used in fabricating microelectronic circuitry.

Simultaneously with the efforts to increase angular resolution, there would be efforts to develop a prototype mirror with a diameter of 1 m. This effort would entail procuring and replicating reflectors from 1-m-diameter mandrels, and fabricating housings of the appropriate dimensions. The housing for the 1-m mirror would likely be designed similarly to housings used for the current narrower conical foil x-ray mirrors, except for modifications needed to attain the required angular resolution.

This work was done by Robert Petre, William Zhang, and Peter Serlemitsos of **Goddard Space Flight Center** *and Yang Soong of USRA.*
GSC-14043

Improved Fiber-Pigtailed Non-Planar Ring Oscillator Laser

Parts are held in stainless-steel housings that are laser-welded together.

NASA's Jet Propulsion Laboratory, Pasadena, California

An improved non-planar ring oscillator (NPRO) of the fiber-pigtailed type has been developed. The improvements over prior lasers of this type lie in details of design and construction that are intended to enhance mechanical stability and thereby increase the stability of optical performance.

A description of the prior art is necessary to put the improvements in perspective: A basic NPRO laser includes a specially shaped laser crystal that serves as the laser cavity. The input and output optical paths in the crystal intersect at a common point on the surface of the crystal. The laser crystal is pumped by a laser diode, the output of which is coupled into the crystal via a cylindrical lens and a grating-index-of-refraction (GRIN) rod lens. Because of the monolithic nature of the laser cavity, the laser frequency is highly stable. Magnets placed near the crystal ensure unidirectional lasing. A quarter-wave plate converts the elliptically polarized output laser beam into a linearly polarized beam, and an optical isolator blocks undesired feedback to the laser. In the case of an NPRO of the fiber-pigtailed type, some components for output coupling to an optical fiber are included in the laser package.

In a fiber-pigtailed NPRO laser package of prior design, all of the aforementioned optical components are mounted, variously, by use of solder, epoxy, or screws on two substrates. In turn, the two substrates are joined to each other by solder at three points. The combination of solder, epoxy, and screws is vulnerable to long-term mechanical instability that can degrade critical alignments of optical components, thereby reducing the net output power.

In the improved NPRO ring laser, the need for critical alignment of the laser-diode pump, lenses, and laser crystal is eliminated because the laser-diode light is coupled to the laser crystal via a bare optical fiber. The NPRO crystal, a heater plate, and a thermistor are placed inside a monolithic, 304L-stainless-steel monolithic block housing by use of a precise tool, then bonded together by use of solder; these are the only components bonded by solder. The other optical components are made with 304L-stainless-steel housings, most of which are laser-welded to the monolithic block housing, except one that is laser-welded to another housing that is, in turn, welded to the monolithic block housing, as described in the next paragraph. Laser welding of these parts is superior to soldering and epoxy bonding and is expected to contribute greater mechanical stability.

In the improved laser as in a typical prior NPRO ring laser, the laser beam is coupled to an output single-mode optical fiber via a GRIN rod lens, which, in this case, is held in a 304L-stainless-steel housing. A novel procedure for alignment of the GRIN rod lens is based on the observation that if the beam is centered on the input face of the lens, then the beam emerges perpendicularly to the output face of the lens. Once the GRIN rod lens has been aligned, its housing is laser-welded to the monolithic block housing. The output optical fiber is held in a ferrule in a housing that, in turn, is laser-welded to the housing of the GRIN rod lens housing. Because the axis of the fiber is held parallel with the output beam emerging from the GRIN rod lens, this arrangement helps to maximize output coupling.

This work was done by Duncan Liu of Caltech for **NASA's Jet Propulsion Laboratory**. *Further information is contained in a TSP [see page 1].*

NPO-20885

Books and Reports

First-Generation Integrated Free-Flying Micro-Spacecraft

The concept of free-flying micro-spacecraft was to develop a miniature spacecraft system fully integrated with a scientific sensor. A fleet of such tiny spacecraft would be deployed in space for multi-probe measurements of a three-dimensional phenomenon and to separate the spatial/temporal variations of that phenomenon. They would measure a parameter of interest, process the data onboard, and communicate the data in real time. In the first-generation proof-of-concept demonstration of free-flying concept, the sensor of choice was a miniature magnetometer and the system was called a Free-Flying Magnetometer (FFM). Two reports describe the design and testing of these free-flying magnetometer systems that were prototypes of future integrated micro-sensor/spacecraft that could be mass-produced in large numbers as expendable units for scientific exploration. The FFMs contained miniature three-axis flux-gate magnetometers plus digital signal processing and data flow control, batteries, clock, attitude determination unit, and communication capabilities. All of this was contained in an FFM "Hockey Puck" with dimensions of 80 mm in diameter and 38 mm height, weighing about 250 g, and having a total power requirement of 1.4 W. The magnetometer had a sensitivity range of 1 to 60,000 nT and a frequency range of 10 mHz to 50 Hz. In a flight test on a sounding rocket (the "Enstrophy" mission), four FFMs were deployed on suborbital trajectories through an aurora and used to study dynamics of magnetic-field-aligned electric-current density in the aurora. This experiment has demonstrated that miniature (<100 g) spacecraft can be designed for simultaneous deployment to measure three-dimensional phenomenon in a local region. One of the key reasons for the success of the FFM mission was the recognition that system requirements could be constrained to fit into the capabilities of a tiny integrated spacecraft.

This work was done by Hamid Javadi, Raymond Goldstein, and James Randolph of Caltech for **NASA's Jet Propulsion Laboratory**. *To obtain copies of the reports, "A Fully Integrated Micro-Magnetometer/Microspacecraft for Multipoint Measurements: The Free-Flyer Magnetometer" and "First-Generation Jet Propulsion Laboratory 'Hockey-Puck' Free-Flying Magnetometers for Distributed In-Situ Multiprobe Measurement of Current Density Filamentation in the Northern Auroral Zone: Enstrophy Mission," see TSP's [page 1].*

NPO-20728

DNS of a Transitional Supercritical C_7H_{16}/N_2 Mixing Layer

This report discusses direct numerical simulations (DNS) of a mixing layer, between a nitrogen stream and a heptane stream initially flowing at different velocities, under supercritical conditions and undergoing a transition to turbulence. Thermodynamically, supercritical conditions prevail when either the temperature or the pressure exceeds its critical value; the critical regime is in particular characterized by the existence of a single phase. The governing conservation equations were formulated according to fluctuation-dissipation (FD) theory, in which the low-pressure typical transport properties (viscosity, diffusivity, and thermal conductivity) are complemented, at high pressure, by a thermal-diffusion factor. The Peng-Robinson equation of state with appropriate mixing rules was coupled to the conservation equations to obtain a closed system. The boundary conditions were periodic in the streamwise and spanwise directions, and of the nonreflecting outflow type in the cross-stream direction. The temperature/pressure regime was one in which both the Kolmogorov and Batchelor scales can be resolved for pseudospecies (species with transport properties modified to enable the attainment of Reynolds numbers large enough for transition). The DNS revealed some of the peculiarities of high-pressure transitional mixing, such as the formation of concentrated regions of high density gradient magnitude wherein the two fluids have difficulty mixing at the molecular level. These regions exhibit strong departures from perfect gas and ideal mixture behavior. Analysis of the DNS database led to several conclusions concerning the inadequacy of the traditional use of the marginal probability density functions of temperature and of species for modeling the reaction rate, which is a joint probability density function. Moreover, it was also found that several probability density functions successful for modeling atmospheric turbulent flow binary mixtures are inadequate for modeling supercritical turbulent mixing.

This work was done by Josette Bellan and Nora Okong'o of Caltech for **NASA's Jet Propulsion Laboratory**. *To obtain a copy of the report, "Direct Numerical Simulation of a Transitional Supercritical Mixing Layer: Heptane and Nitrogen," see TSP's [page 1].*

NPO-21144

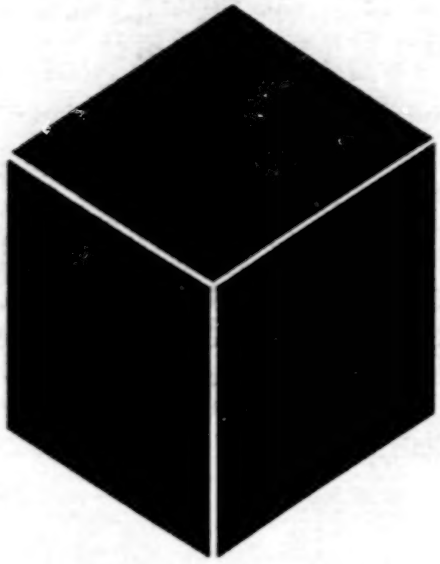

Materials

Hardware, Techniques, and Processes

21 End Caps Increase Thermo-Oxidative Stability of Polyimides
22 End Caps for More Thermo-Oxidative Stability in Polyimides
23 Low-Density, Ablative Resin-Impregnated Ceramic Insulation
24 Solar Heating for Deployment of Foam Structures
24 Fluorinated Diamondlike Carbon Coatings

Books and Reports

25 Solar Sails Would Be Made From Carbon Nets
25 Solar Sails Would Be Segmented To Minimize Stresses

BLANK PAGE

End Caps Increase Thermo-Oxidative Stability of Polyimides

A thermo-oxidative-reaction path that leads to more stable products is exploited.

John H. Glenn Research Center, Cleveland, Ohio

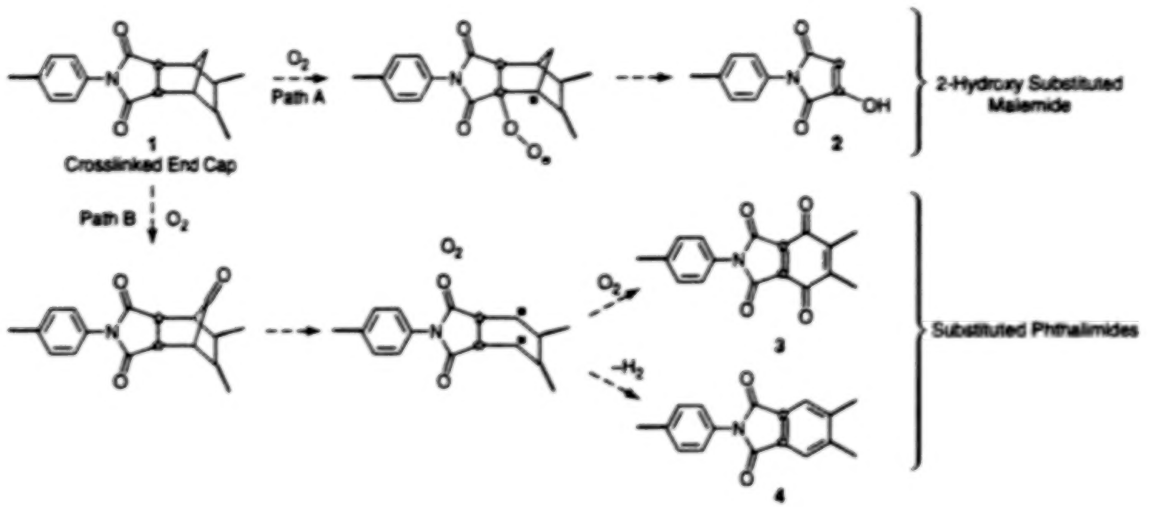

Figure 1. The Thermo-Oxidative Degradation of a norbornenyl end cap follows paths A and B. The products of path B are more stable than are those of path A.

Latently reactive end caps have been investigated as improved means to increase the thermo-oxidative stability of polyimides of the polymerization of monomeric reactants (PMR) type, which are often used as the matrix resins of high-temperature-resistant composite materials. The present end-cap compounds are candidates to supplant the norbornene end cap (NE) compound that, heretofore, has served to limit molecular weights during oligomerization and, at high temperatures, to form crosslinks that become parts of stable network molecular structures.

NE has been important to processability of high-temperature resins because (1) in limiting molecular weights, it enables resins to flow more readily for processing and (2) it does not give off volatile byproducts during final cure and, therefore, enables the production of void-free composite parts. However, with respect to ability of addition polymers to resist oxidation at high temperature, NE has been a "weak link." Consequently, for example, in order to enable norbornene-end-capped polyimide matrices to last for lifetimes up to 1,000 hours, it is necessary to limit their use temperatures to ≤315 °C. The present improved end caps are also subject to oxidation at high temperature, but they oxidize in a different manner, such that the long-term stability of a polymer made with one of these end caps exceeds the long-term stability of the corresponding polymer made with NE. Hence, use temperatures and/or lifetimes can be increased.

Prior attempts to increase thermo-oxidative stability of PMR polyimides were oriented toward formulation of end caps that are inherently more stable than is the nadic end cap. The results were not satisfactory in that the end caps thus formulated adversely affected processability, the nature of the crosslinks, and, in some cases, the thermomechanical properties of the resulting polymers. In the present approach, one does not attempt to formulate end caps that are inherently more stable; instead, one seeks nadic derivatives that exploit one of the modes of the thermo-oxidative degradation of the nadic end cap in such a way as to retard the overall thermo-oxidative degradation of the affected polymers.

Research on the aging of PMR-15 polyimide has revealed that the degradation of the nadic end cap can occur via two primary reaction paths, designated A and B (see Figure 1). On path A, degradation proceeds through initial scission and oxidative opening of the norbornyl ring to form a 2-hydroxy substituted maleimide. On path B, degradation proceeds through oxidation of the bridging methylene of the norbornene moieties, followed by carbon monoxide extrusion. Aromatization of the resulting biradical leads to substituted phthalimides, and related secondary degradation products. The oxidation products of path A (including the 2-hydroxy substituted maleimide) are cleavage products that are most likely formed concomitantly with large loss of weight from the affected polymer. In contrast, the products of path B are more oxidatively stable and form with very little weight loss.

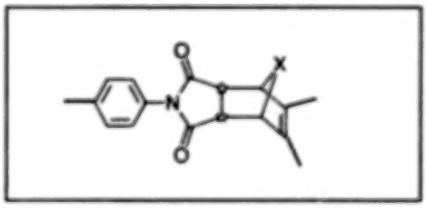

Figure 2. End Caps of This Molecular Structure have been investigated for their potential to increase the thermo-oxidative stability of polyimides. X can be CRR′, where R or R′ can be H, OH, SH, F, Cl, an alkyl, an alkoxy, or an aryl; alternatively, X can be a ring molecular substructure.

Therefore, in the present approach, one seeks to formulate end caps that preserve desirable processing properties of NE while favoring path B strongly, leading to lower weight loss and thus less shrinkage and cracking in the thermally oxidized layer of the affected polymer. Figure 2 depicts a generic molecular structure for a class of end caps that become thermo-oxidatively degraded primarily along path B. In this structure,

X maintains its stability during imidization (at a temperature of 200 °C) and cross-linking (at 315 °C). Nevertheless, following these critical steps, X is spontaneously converted, upon aging, to a thermally stable capping group.

This work was done by Mary Ann B. Meador and Aryeh A. Frimer of **Glenn Research Center**. *Further information is contained in a TSP [see page 1].*

Inquiries concerning rights for the commercial use of this invention should be addressed to NASA Glenn Research Center, Commercial Technology Office, Attn: Steve Fedor, Mail Stop 4–8, 21000 Brookpark Road, Cleveland, Ohio 44135. Refer to LEW-16987.

End Caps for More Thermo-Oxidative Stability in Polyimides

Alternatives to previous formulations have been found.

John H. Glenn Research Center, Cleveland, Ohio

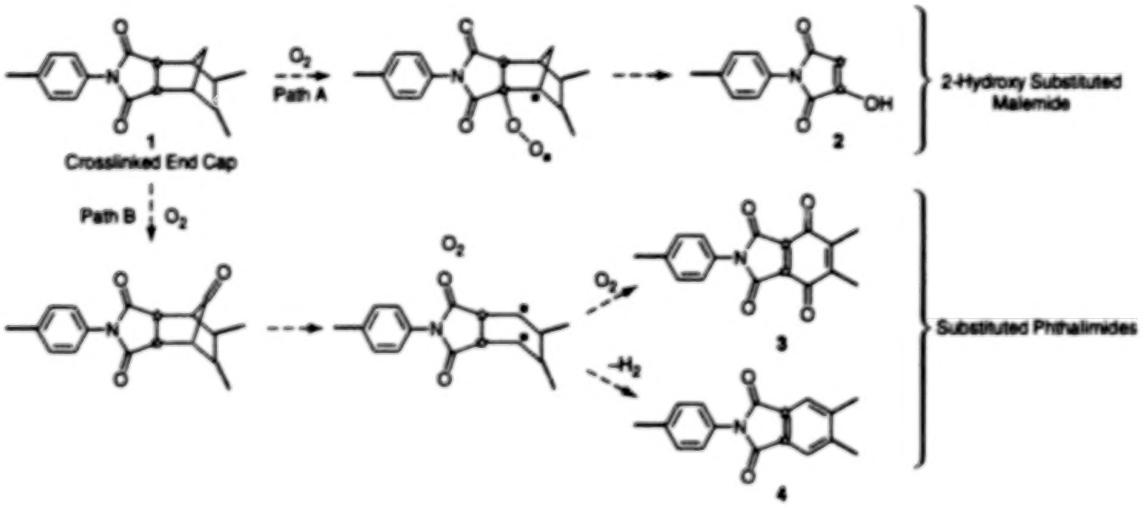

Figure 1. The Thermo-Oxidative Degradation of a norbornenyl end cap follows paths A and B. The products of path B are more stable than are those of path A.

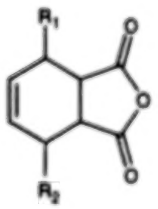

Figure 2. End Caps of This Molecular Structure are alternatives to previously reported end caps for increasing the thermo-oxidative stability of polyimides. R_1 or R_2 or both can be alkyl, alkoxy, aryl, flouro, chloro, carbomethoxy, nitro, or another substituent.

An additional class of end-cap compounds that increase the thermo-oxidative stability of polyimides of the polymerization of monomeric reactants (PMR) type has been invented. The prior class of end-cap compounds in this line of development was described in "End Caps Increase Thermo-Oxidative Stability of Polyimides" (LEW-16987), this issue, page 21.

PMR polyimides are often used as matrix resins of high-temperature-resistant composite materials. Like the end-cap compounds described in the cited previous article, the present end-cap compounds are candidates to supplant the norbornene end cap (NE) compound that, heretofore, has served to limit molecular weights during oligomerization and, at high temperatures, to form cross-links that become parts of stable network molecular structures.

To recapitulate from the cited previous article: NE has been important to processability of high-temperature resins because (1) in limiting molecular weights, it enables resins to flow more readily for processing and (2) it does not give off volatile byproducts during final cure and, therefore, enables the production of void-free composite parts. However, with respect to ability of addition polymers to resist oxidation at high temperature, NE has been a "weak link." Consequently, for example, in order to enable norbornene-end-capped polyimide matrices to last for lifetimes up to 1,000 hours, it is necessary to limit their use temperatures to ≤315 °C.

Like NE and like the end caps described in the prior article, the present end caps are also subject to oxidation at high temperature, but they oxidize in a different manner, such that the long-term stability of a polymer made with one of these end caps exceeds the long-term stability of the corresponding polymer made with NE. Hence, use temperatures and/or lifetimes can be increased.

Prior to the present line of development, attempts to increase thermo-oxidative stability of PMR polyimides were oriented toward formulation of end caps that are inherently more stable than is the nadic end cap. The results were not satisfactory in that the end caps thus formulated adversely affected processability, the nature of the cross-links, and, in some cases, the thermomechanical properties of the resulting polymers. In the present approach, one does not attempt to formulate end caps that are inherently more stable; instead, one seeks derivatives that exploit one of the modes of the thermo-oxidative degradation of the nadic end cap in such a way as to retard the overall thermo-oxidative degradation of the affected polymers.

Research on the aging of PMR-15 polyimide has revealed that the degradation of the nadic end cap can occur via two primary reaction paths, designated A and B (see Figure 1). On path A, degradation proceeds through initial scission and oxidative opening of the norbornyl ring to form a 2-hydroxy substituted maleimide. On path B, degradation proceeds through oxidation of the bridging methylene of the norbornene moieties, followed by carbon monoxide extrusion. Aromatization of the resulting biradical leads to substituted phthalimides, and related secondary degradation products. The oxidation products of path A (including the 2-hydroxy substituted maleimide) are cleavage products that are most likely formed concomitantly with large loss of weight from the affected polymer. In contrast, the products of path B are more oxidatively stable and form with very little weight loss and with less shrinkage and cracking in the oxidized layer.

The present end caps are formulated to preserve the desirable processing properties of NE and to undergo thermo-oxidative degradation primarily or exclusively along path B. Figure 2 depicts a generic molecular structure for the present class of end caps. In this structure, the end cap contains no bridging methylene. Rather, the end cap is a 1,2,3,6-tetrahydrophthalic anhydride, substituted in such a way as to lower the cross-linking temperature from >415 °C to between 280 and 350 °C. The end cap maintains its stability during imidization (at 200 °C) and cross-linking. After the foregoing critical steps, the end cap is spontaneously converted, upon aging, to thermally stable capping groups.

This work was done by Mary Ann B. Meador of **Glenn Research Center**. *Further information is contained in a TSP [see page 1].*

Inquiries concerning rights for the commercial use of this invention should be addressed to NASA Glenn Research Center, Commercial Technology Office, Attn: Steve Fedor, Mail Stop 4–8, 21000 Brookpark Road, Cleveland, Ohio 44135. Refer to LEW-17012.

Low-Density, Ablative Resin-Impregnated Ceramic Insulation

Properties can be tailored for enhanced thermal protection.

Ames Research Center, Moffett Field, California

Low-density, ablative thermal-protection panels can be made by impregnating fibrous ceramic substrates with organic polymers. With proper design and fabrication, these panels can protect temporarily against temperatures up to 3,500 °C or heat fluxes up to 16 MW/m^2.

Like ablative thermal-protection panels of older types made of other combinations of materials, the panels of the present type absorb and dissipate incident heat through depolymerization and charring of resins, transpiration (blowing of gaseous pyrolysis products from boundary layers), and radiation from charred surface layers. In comparison with panels of older types, the panels of this type are more porous; thus, gaseous pyrolysis products can percolate more freely. The panels of the present type also dissipate heat through additional mechanisms that can include vaporization of ceramic fibers and radiation from the heated surfaces of the ceramic substrates.

At a heat flux in the approximate range of 1 to 2.5 MW/m^2, the surface layer that forms on a typical panel of the present type includes not only a char formed by decomposition of the organic material but also the coalesced ends of ceramic fibers. The resulting char layer that builds up on the surface is stronger than are the char layers that build up on ablative thermal-protection panels of older types, and the surface-recession rate for this panel is therefore lower.

Another contribution to thermal protection arises from a complex of additional mechanisms that also occur at a heat flux in the approximate range of 1 to 2.5 MW/m^2:

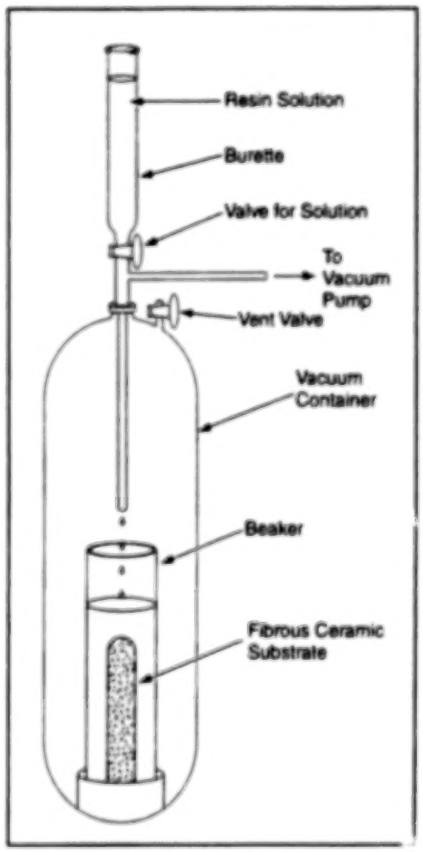

The Fibrous Ceramic Substrate Is Impregnated with the resin solution in this apparatus. The impregnated substrate is then processed further to obtain a porous fibrous ceramic panel, the fibers of which are coated with a polymer.

If, for example, the ceramic fibers are made of silica, then during pyrolysis, the organic material can react with the fibers to form a layer of silicon carbide protected by a thin, glassy layer of silicon dioxide. The glassy layer makes the panel less catalytic and thereby reduces the rate of convective heating. The surface is also highly emissive and therefore most of the energy absorbed at the surface is reradiated. The combination of reduced convective heating and reradiation helps to suppress loss of mass and recession of the surface.

At a heat flux in the approximate range of 4.3 to 16 MW/m^2, the panel dissipates incident heat almost entirely by reradiation and micro spallation or evaporation of the ceramic substrate. The combination of a resin that has a high char yield and a substrate that has a high melting temperature enables the panel to reradiate heat efficiently from the heated surface without undergoing melting or significant mechanical failure.

Fibrous substrates for these panels can be made of any of a variety of ceramic materials; for example, silica (mentioned above), zirconia, boria, hafnia, or silicon carbide, to name a few. Organic materials suitable for infiltration into the substrates include thermoplastic and thermosetting resins. Substrates can be impregnated evenly throughout their thicknesses; alternatively, by suitable design of infiltration processes, one can obtain gradients in the densities of the polymers.

The figure illustrates an apparatus and process for impregnating a ceramic substrate with a resin. The burette on top of the vacuum chamber is initially filled with a resin solution. Also initially, the beaker in the vacuum container is empty. The substrate is placed in the beaker, then the chamber is evacuated, then the solution is allowed to

flow into the beaker until the substrate is entirely immersed. Then the chamber is disconnected from the vacuum pump and vented to the atmosphere, forcing the solution into the interstices of the substrate.

Next, the impregnated substrate is removed from the beaker and subjected to further processing that depends on the type of resin and the desired uniformity or gradient of density; for example, to achieve even impregnation with a thermoplastic resin, the substrate can be dried slowly in air. When processing is complete, the fibers are coated with a primer. Typically, the resulting panel has a void volume fraction between 85 and 93 percent, a density between 0.17 and 0.3 g/cm^3, and a resin content between 30 and 60 weight percent.

This work was done by Huy K. Tran, William D. Heinline, Ming-ta S. Hsu, Daniel J. Rasky, and Salvatore R. Ricciello of **Ames Research Center**. *Further information is contained in a TSP [see page 1].*

This invention has been patented by NASA (U.S. Patent No. 5,672,389). Inquiries concerning nonexclusive or exclusive license for its commercial development should be addressed to the Patent Counsel, Ames Research Center, (650) 604-5104. Refer to ARC-12011-2.

Solar Heating for Deployment of Foam Structures

Local sources of energy could be reserved for other purposes.

NASA's Jet Propulsion Laboratory, Pasadena, California

Solar heating has been proposed as a means of deployment of structures of the type described in "Cold Hibernated Elastic Memory (CHEM) Expandable Structures," (NPO-20394), *NASA Tech Briefs*, Vol. 23, No. 2 (February 1999), page 56. A few examples of structures that would be amenable to the CHEM approach include expandable shelters, tanks, rafts, and thermally insulating boxes for storing food and drinks.

To recapitulate from the cited prior article: The CHEM concept is one of utilizing open-cell foams of shape-memory polymers (SMPs) to make lightweight, reliable, simple, and inexpensive structures that can be alternately (1) compressed and stowed compactly and later (2) expanded and rigidified for use. A CHEM structure of any shape is compacted to a small volume while in the rubbery state above the glass-transition temperature (T_g) of the SMP. After compaction, the structure is cooled below T_g where it is frozen in the glassy state of the SMP. The compacting force can then be released and the structure remains compact as long as the temperature is kept below T_g. Upon subsequent heating of the structure above T_g to the rubbery state of the SMP, the simultaneous elastic recovery of the foam and its shape-memory effect cause the structure to expand to its original size and shape. Once thus deployed, the structure can be rigidified by cooling below T_g to the glassy state. Once deployed and rigidified, the structure could be heated and recompacted. In principle, there should be no limit on the achievable number of compaction/deployment/rigidification cycles.

The attractiveness of the CHEM structure is the wide range of T_g resulting in a variety of potential space and terrestrial applications. Experiments have confirmed the feasibility of this innovative, self-deployable, and rigidizable structure.

The disadvantage of CHEM structures is that heat is needed for deployment. The proposed use of solar heat would eliminate the need to deplete other energy sources. According to the proposal, a CHEM structure would be wrapped in a blanket made of a material with a high ratio between solar absorptivity and infrared emissivity. Upon exposure to solar radiation, the structure inside the blanket would become heated because the blanket would absorb more heat than it would reradiate. Eventually, the temperature of the wrapped structure would increase beyond T_g, causing the structure to deploy itself by expanding to its full size and shape. After full deployment, the blanket would be removed, causing the structure to become cooled below T_g and thus rigidified. Thermal analysis confirmed a feasibility of this concept in the Mars environment. This concept will also work for applications on Earth and perhaps perform even better than on Mars.

This work was done by Witold Sokolowski, Art Chmielewski, and Henry Awaya of Caltech for **NASA's Jet Propulsion Laboratory**. *Further information is contained in a TSP [see page 1].*
NPO-20961

Fluorinated Diamondlike Carbon Coatings

This material is expected to exhibit low friction and resistance to atomic oxygen.

Lyndon B. Johnson Space Center, Houston, Texas

Some experiments directed toward the development of improved hard, lubricious coating materials have involved direct fluorination of proprietary diamondlike coats on various substrates. The idea is to retain the hardness of the diamondlike material while adding surface molecular structures that impart the chemical inertness (especially resistance to erosion by atomic oxygen) and lubricity of fluorinated polymers.

The proprietary diamondlike coating material is Amorohic Diamond™, which comprises nodules of carbon that have the molecular/crystalline structure of diamond, with sizes of 100 to 200 nm, densely and uniformly packed in a net of amorphous carbon polytypes. This material has a low coefficient of friction and is almost as hard as diamond is. However, it is not brittle: it can withstand flexure or shock without cracking. It can be applied to plastic, polymer, metal, and ceramic substrates.

In the experiments reported thus far, material samples coated with the diamondlike material were exposed to fluorine to create a surface layer of highly inert carbon/fluorine molecular bonds. Fluorination did not degrade the lubricity and hardness of the diamondlike coats. Among the samples were sheets of Kapton™ polyimide 5 mils (about 0.1 mm) thick. The sheets remained flexible after fluorination of the diamondlike coats. The coating layers were not compromised, even when the sheets were creased.

At the time of submission of information for this article, the ability of the fluorinated coats to resist erosion by atomic oxygen remained untested. Also untested at that

time was the combined effect of ultraviolet radiation and erosion by atomic oxygen (this is of concern because the rates of erosion of fluoropolymers by atomic oxygen have been observed to increase in the presence of vacuum ultraviolet radiation).

This work was done by Mark S. Hammond and A. Wesley Moorehead of SI Diamond Technology, Inc., for **Johnson Space Center**. *Further information is contained in a TSP [see page 1].*
MSC-22364

Books and Reports

Solar Sails Would Be Made From Carbon Nets

A report proposes that solar sails for spacecraft be made from nets of carbon fibers. The reason for choosing carbon nets over thin polymeric films is that nets offer greater capability for carrying tensile loads. The sails could be made from carbon-fiber nets of various thicknesses: nets used for high emissivity could be made from nanotube carbon fibers; nets for holding aluminum reflectors could be made from micron-thickness fibers; nets to carry tensile loads in sails could be made from fibers with thicknesses between 10 and 100 μm; and nets to carry large bulk loads and loads in high-stress areas could be made from fibers with thicknesses from 100 to 1,000 μm.

This work was done by Charles Garner of Caltech for **NASA's Jet Propulsion Laboratory**. *To obtain a copy of the report, "Carbon Net Solar Sail," see TSP's [page 1].*
NPO-20852

Solar Sails Would Be Segmented To Minimize Stresses

A report proposes that solar sails for spacecraft be constructed in segments in such a way as to minimize stresses. The segments could be made of metallized fabric or film and could be connected by short, strong tethers. Alternatively, the segments could be like islands, held loosely in pockets bounded by fibers. For stowage during transport to outer space, the sails could be folded along the gaps between segments, so as to minimize folding stresses in the sail material. Because tensile and other stresses in the sail material would be minimal, the sail material could be made in a thickness of the order of a micron and could thus be very lightweight. In cases in which there are requirements for sails to sustain tensile stresses, carbon-fiber nets like those described in the preceding article could be used.

This work was done by Charles Garner of Caltech for **NASA's Jet Propulsion Laboratory**. *To obtain a copy of the report, "Segmented Solar Sail Design," see TSP's [page 1].*
NPO-20853

BLANK PAGE

Computer Programs

Physical Sciences

29 Advanced Software for Two-Phase Thermohydraulic Systems
29 Software for Simulation of 3D, Three-Phase Combusting Flow
30 Computing Atmospheric Profiles From Spectral Measurements

Mechanics

30 Software for Selecting Modes of Vibration of a Structure

Mathematics and Information Sciences

30 Software for Concurrent Development of Reusable Software
31 Adaptive Problem Solving for Refining Control Strategy
31 Software for Automated Ortho-Rectification of SAR Images
31 Test Automation Software for AI Planning Software

BLANK PAGE

Physical Sciences

Advanced Software for Two-Phase Thermohydraulic Systems

Recent improvements in the SINDA/FLUINT computer program have made the program into a highly capable, commercially viable software product for general mathematical modeling of thermohydraulic systems. Versions of SINDA/FLUINT have been described in a number of previous *NASA Tech Briefs* articles. To recapitulate: SINDA/FLUINT is the NASA standard software system for computational simulation of interacting thermal and fluid effects in arbitrary flow networks. As its name suggests, SINDA/FLUINT is an integral combination of two subprograms: Systems Improved Numerical Differencing Analyzer (SINDA) program is a software system for solving lumped-parameter representations of physical problems governed by diffusion-type equations. The Fluid Integrator (FLUINT) program is an advanced one-dimensional fluid-analysis program that solves equations of arbitrary fluid-flow networks. Working fluids that can be modeled in SINDA/FLUINT include single-phase vapors, single-phase liquids, and two-phase fluids.

The recent improvements in SINDA/FLUINT fall into two categories. In the first category is the addition of capabilities for advanced mathematical modeling of two-phase flows of types that are of particular relevance to thermal-control, propulsion, environmental-control, and fire-suppressant-delivery systems. Phenomena that could not previously be modeled but can now be modeled include the dissolution and evolution of noncondensable gases and the effects of thermal equilibrium between the liquid phase and the vapor/gas phase in a pipe. Specific features added to the program include one that defines the equilibrium dissolution of a solvent/solute pair, mass-transfer correlations based on flow regime, a feature for tracking of solutes and rates of evolution and dissolution in both tank and junction network elements, interface network elements to provide for subdivision of control volumes, twinned tanks, twinned ties, and superpaths.

The second category of improvements comprises miscellaneous additions that provide enhanced capabilities for posing and solving problems. The additions include (1) prepackaged software components that provide options for handling ducts with axially varying flow areas, (2) software components that provide double-precision solution options, (3) software components that implement some optional solution techniques, and (4) a database subprogram that manages complex relationships among inputs and outputs and represents these relationships in a spreadsheet. The latter improvement relieves the user of some programming tasks, making parametric analyses easy and making the program easier to learn and to apply to complex problems.

This program was written by Brent Cullimore, David A. Johnson, and Steven G. Ring of Cullimore and Ring Technologies, Inc., for **Johnson Space Center**. *Further information is contained in a TSP* *[see page 1]*.

MSC-23052/58

Software for Simulation of 3D, Three-Phase Combusting Flow

A computational fluid dynamics (CFD) code has been developed to enable simulation of spray combustion near the fuel injectors in a liquid-fueled rocket engine. This code reflects the three-dimensional (3D), multiphase nature of the flow field in a rocket engine and is capable of modeling even a flow field as complex as one that results from the use of impingement injectors. Unlike prior spray-combustion codes that emphasize physical constraints at the expense of geometric ones, this code implements a compromise between physical and geometric constraints in order to enable analysis and comparison of the performances of alternative engine designs that involve different injector geometries. In particular, this code was constructed to enable prediction of the interactive effects of injector-element impingement angles and impingement points, momenta of individual orifice flows, and the resulting combusting flow.

This computer program includes finite-difference Navier-Stokes CFD subprograms for mathematical modeling of spray combustion from several different perspectives. Two of the subprograms implement models of heterogeneous spray combustion: One of these models, denoted a volume-of-fluid (VOF) model, represents a liquid core of coaxial and impinging jets and the atomization and vaporization thereof. The other, denoted a blob model, represents injected streams as a cloud of droplets that are initially of the size of the injector orifice and that subsequently exhibit particle interaction, vaporization, and combustion. These models are computationally intensive, as they must be to account accurately for the complex combustion and other physics that one seeks to predict.

One of the subprograms implements a model of homogeneous spray combustion, representing the flow as a continuum of multiphase, multicomponent fluids that move without thermal or velocity lags among the phases. This model enables relatively fast computation. To enable the representation of subcritical and supercritical liquid and vapor flows, this subprogram uses a real-fluid model that comprises thermal and caloric equations of state. The great advantage of this real-fluid model is that it is valid over a wide range of pressures and temperatures, making it unnecessary to provide (as in prior approaches) a submodel to represent the effects of surface tension in the subcritical regime; this is important because liquid-fuel rocket engines usually operate at supercritical pressures (for which surface tensions are zero), making it counterproductive to continue to adapt low-pressure spray-combustion models.

Because some rocket engines utilize RP-1 (essentially, kerosine) and liquid oxygen as propellants, the homogeneous-spray subprogram includes a simplified hydrocarbon-combustion model for use in simulations of 3D, multiphase flow. This model does not identify drops or their distribution, but it does enable accurate prediction of film coolant flow and of recirculating flow along the injector face and into an acoustic cavity. Soot is represented as a third phase that behaves as a dense gas. The resolution of the flow field of the reacting, vaporizing propellants predicted by this spray model exceeds that of any other published model developed for the same purpose.

The heterogeneous VOF and blob spray-combustion subprograms include provisions for Euler-Lagrange particle tracking to account for thermal and velocity lag of droplets. These subprograms also use the real-fluid equations of state to calculate thermodynamic properties of fluids.

This program was written by R. C. Farmer and G. C. Cheng of SECA, Inc.,

and Y. S. Chen of Engineering Sciences, Inc., for **Marshall Space Flight Center**. *Further information is contained in a TSP [see page 1].*
MFS-31599

Computing Atmospheric Profiles From Spectral Measurements

The SEASCRAPE computer program estimates the composition, temperature, and pressure of the atmosphere as a function of position by fitting remote-sounding spectroscopic data to a mathematical model of the transfer of radiation through the atmosphere. SEASCRAPE consists of two integrated parts: (1) A forward mathematical model that is used to generate synthetic spectra and (2) an inversion algorithm that is used to estimate parameters. The forward model evaluates the emission and absorption of radiation on a line-by-line basis; in its current form, it includes a one-dimensional (spherically symmetrical) atmospheric submodel with homogeneous layers of arbitrary thickness. A future version of the code will include a multidimensional submodel with inhomogeneous cells. The inversion algorithm uses a sequential parameter-estimation method known as the square-root information filter. The program incorporates some flexibility for handling large sets of data; the user can control the level of accuracy in the model equations for spectral lines to trade accuracy against speed. The program can run on a single processor but is written for a parallel-processing environment; if a parallel processor is available, it can simultaneously retrieve multiple distributions and/or estimate a single set of parameters from multiple spectra.

This program was written by Lawrence Sparks, James McComb, and John L. Fanselow of Caltech for **NASA's Jet Propulsion Laboratory**. *Further information is contained in a TSP [see page 1].*

This software is available for commercial licensing. Please contact Don Hart of the California Institute of Technology at (818) 393-3425. Refer to NPO-19694.

Mechanics

Software for Selecting Modes of Vibration of a Structure

A computer program facilitates the selection of the dominant modes of vibration of a structure — especially the dominant modes that interact with specific locations on the structure. This program is intended for use in conjunction with any of the various vibration-mode-analysis programs based on the finite-element method (FEM). The program was written to satisfy a need to accurately and quickly sort through enormous amounts of information about the vibrational modes of the developmental X-33 aerospace launch vehicle in order to select the dominant modes and thereby reduce the subsequent computational burden of analyzing the vibrations of the vehicle. In the X-33 application, the program has been used to determine which modes interact most with specific locations and pieces of equipment that affect and are affected by stability or instability with respect to (1) flight control and (2) a phenomenon, called "pogo" (because it is reminiscent of oscillations like those of a pogo stick), which involves deformations of liquid-oxygen plumbing combined with sloshing and/or fluctuations in pressure of the liquid oxygen inside the plumbing. The program could also be adapted for use in analyzing the vibrations of structures other than that of the X-33.

The system of dynamical equations that describe the undamped free vibrations of a structure yields a set of roots or eigenvalues, which in turn, determine a set of natural mode shapes or eigenvector coefficients. Because the equations are homogenous, there is not a unique solution for the eigenvector coefficients; one can obtain only ratios among the eigenvector coefficients. The shape of a given mode is defined by the ratios among the amplitudes of the motion that occurs at the various points on the structure when the structure is excited at the natural frequency of that mode. If one of the elements of the eigenvector is assigned a certain value, the rest of the elements of the same eigenvector are also fixed because the ratio between any two elements is constant.

The present computer program takes advantage of the facts presented in the preceding paragraph. The program is based partly on the use of orthonormal modes and partly on the root-sum-square (RSS) measure of the modes that affect each degree of freedom (DOF) in the FEM dynamical model of the structure. The displacements in all modes for all DOFs are normalized to the unity of the largest eigenvector displacement.

With the help of this program, one can make a direct comparison between modes for a particular location. The program computes magnitudes of the resultant displacement values for each mode at selected DOFs and sorts to locate modes with highest values. The modes with the highest RSS displacement values are deemed to have the highest overall motion and kinetic energy for the given location or node. Then by keying on the RSS displacement values for locations of interest, one can easily filter out thousands of modes that are not of interest, leaving only the modes of interest.

The program also sums the absolute displacement along the three coordinate axes for each mode. Again, the program sorts to locate modes with highest values. The result of this sorting process yields insight into the directional dynamic behavior of the modes. This aspect of the program can be used, for example, to identify the pogo modes as those for which the longitudinal (*x*) axis yield the highest values.

This program was written by Homero Hidalgo of **Marshall Space Flight Center**. *For further information, access the Technical Support Package (TSP)* ***free on-line at www.nasatech.com*** *under the category.*
MFS-31466

Mathematics and Information Sciences

Software for Concurrent Development of Reusable Software

The YaM computer program provides a conceptual framework (including configuration management) and a set of software tools that support the concurrent development of reusable software by members of a team. YaM favors development of software in modules that can be assembled into packages and that, during development, serve collectively as the software analog of scaffolding that supports the development of other modules. YaM is written in Practical Extraction and Reporting Language (PERL) and is organized as a set of software utilities on top of the public-domain Concurrent Versioning System (CVS) software. Programmers can set up sandboxes for the development of modules and packages: all such development takes place on private CVS branches. High-level YaM commands support the setup, update, and release of modules and packages. Released and prebuilt versions of modules are available to all programmers on the team. Programmers can tailor the mixes of source and link modules for their sandboxes so that new sandboxes can be built up easily and quickly by pointing to previously released modules. All intermodule interfaces are publicly exported via links. A minimal, but uniform, con-

vention is used for building modules.

This program was written by Abhinandan Jain and Jeffrey Biesiadecki of Caltech for **NASA's Jet Propulsion Laboratory**. *Further information is contained in a TSP [see page 1].*

This software is available for commercial licensing. Please contact Don Hart of the California Institute of Technology at (818) 393-3425. Refer to NPO-21083.

Adaptive Problem Solving for Refining Control Strategy

A computer program implements an adaptive problem-solving (APS) algorithm for real-time development, refinement, and maintenance of the control strategy of an autonomous system that must operate in an environment about which little or no detailed information is available in advance. In the initial application for which the APS software was developed, the autonomous system would be an exploratory spacecraft that would feature a flexible control architecture and would be equipped with planning and scheduling software, which the APS software would complement. Given a generic set of control strategies, the APS software evaluates the strategies, performs "what-if" analyses, and utilizes statistical methods to rank each strategy or generate a more appropriate strategy in face of current information about the environment. In an iterative process of reinforcement learning, the highest-ranked strategies are passed back and forth between the APS algorithm and a search algorithm until a stopping criterion is satisfied. The user can specify the allowable error in the choice of the best control strategy. In this choice, other things being equal, strategies that can be evaluated accurately by use of fewer data points are favored over those for which more data points are needed.

This program was written by Steve Chien, Barbara Engelhardt, Darren Mutz, and Robert Sherwood of Caltech for **NASA's Jet Propulsion Laboratory**. *Further information is contained in a TSP [see page 1].*

This software is available for commercial licensing. Please contact Don Hart of the California Institute of Technology at (818) 393-3425. Refer to NPO-21071.

Software for Automated Ortho-Rectification of SAR Images

The Automated SAR Ortho-rectification Software System enables users of synthetic-aperture-radar (SAR) data to form processed images that are free of the distortion caused by the SAR imaging geometry and topography. The software consists of four modules:

- FOCUS™, a program for automated formation of SAR images;
- PHASE™, a complete package of software for interferometry;
- RadarStereo™, a stereoscopic-image-processing program; and
- OrthoSAR™, a package of software for automated terrain and geometry correction and geocoding of SAR image data.

The disadvantage of SAR satellite data is that heretofore, images obtained by processing the data have been distorted by the peculiar imaging geometry of SAR systems and by topography. However, SAR can provide information that is not obtainable by other imaging techniques. Because SAR is unaffected by clouds, digital elevation models (DEMs) can always be obtained by use of stereoscopic SAR. Furthermore, because SAR is a coherent imaging technique, accurate DEMs can be obtained by use of interferometry; these accurate topographic models can be used by OrthoSAR™ to remove from imagery the distortion due to topography and imaging geometry.

Techniques for processing SAR image data, including techniques for processing data from stereoscopic and interferometric SAR, and techniques for ortho-rectification, existed before the development of the present software. However, there were no commercial-grade software systems for stereoscopy and ortho-rectification, and there was no integrated system that performed all of these functions.

The principal novelty of this software is the integration, into one easy-to-use package, of all of the software packages needed to process SAR data, including the processing to extract DEMs and the distortions due to imaging geometry and topography. The modules were designed and implemented in an object-oriented manner so that they can easily be upgraded as new techniques or new data sources become available. The software system was constructed to be operated through a Java™ graphical user interface, which can also be easily changed and upgraded as needed.

FOCUS™ is fully automated, can be used to process data from all current SAR satellite missions, and can easily be modified to work with data from future missions. The software is able to take advantage of multiprocessor architectures and is significantly faster than previously available software designed for the same purpose.

PHASE™ can be used to create DEMs with vertical errors of less than a meter (depending on the quality of the data). In the displacement-map mode, PHASE™ can be used to detect tectonic movement or subsidence of the ground to a sensitivity of less than a centimeter. While the software affords much flexibility in process control, including choice among different algorithms for several of the necessary tasks, it remains easy to use. A particular advantage of the software is that a crude DEM, perhaps one that was created with RadarStereo™, can be ingested to aid in the production of a more accurate, refined DEM.

RadarStereo™ is fully automated and uses novel techniques for the registration of images and generation of tie points. It also uses a novel algorithm for calculating stereoscopic solutions from radar parameters.

OrthoSAR™ is also fully automated, and, unlike other ortho-rectification software packages, it uses the radar equations to perform corrections. OrthoSAR™ can optionally produce a mask of regions where imagery is compromised by layover or by shadow.

Significant interest in this integrated software system has been expressed by persons in universities and laboratories who wish to use the software to create DEMs to study motion and deformation of the ground. Some features of this software are also being marketed as part of a comprehensive radar ground station, with great success. OrthoSAR™ and RadarStereo™ are also available as parts of a popular geographic-information software system, ERDAS Imagine™.

This work was done by Grant R. Burkhart of Vexcel Corp. for **Stennis Space Center**. *For further information, please contact Ron McCoy, (303) 444-0094, extension 229.*

In accordance with Public Law 96-517, the contractor has elected to retain title to this invention. Inquiries concerning rights for its commercial use should be addressed to

Vexcel Corporation
22477 55th Street
Suite 201
Boulder, CO 80301

Refer to SSC-00108, volume and number of this NASA Tech Briefs *issue, and the page number.*

Test Automation Software for AI Planning Software

This test automation software reduces the burden of testing artificial-intelligence (AI) planning software written in the Heuristic Scheduling Testbed System (HSTS) [a software architecture for planning and scheduling]. It automates what would otherwise be the labor intensive and infeasibly time-consuming process of determining whether the plans produced by the planner in response

to test case inputs are consistent with the specifications. Automating this process is particularly important for verifying planning systems due to the large numbers of test cases and the complexity of both the plans and the specifications. This program automatically translates constraints written in the HSTS constraint language into automatically executable queries in a database language. As a result, plans generated by HSTS planning software can be automatically verified for satisfaction of all the constraints. Moreover, the constraints can be validated by manually expressing their intents directly in the database query language, then plans generated by the HSTS planning software can be automatically verified through the responses to those queries. Redundant information contained within plans is automatically cross-checked, thus increasing confidence in the correct operation of the planning software and of the plan-checkers themselves. This program generates a pass/fail report of the responses of the planning software, as well as detailed and summary reports as to how each constraint was or was not satisfied. It also generates simple metrics concerning the constraints and requirements exercised in testing.

This program was written by Benjamin Smith and Martin Feather of Caltech for **NASA's Jet Propulsion Laboratory**. *Further information is contained in a TSP [see page 1].*

This software is available for commercial licensing. Please contact Don Hart of the California Institute of Technology at (818) 393-3425. Refer to NPO-21118.

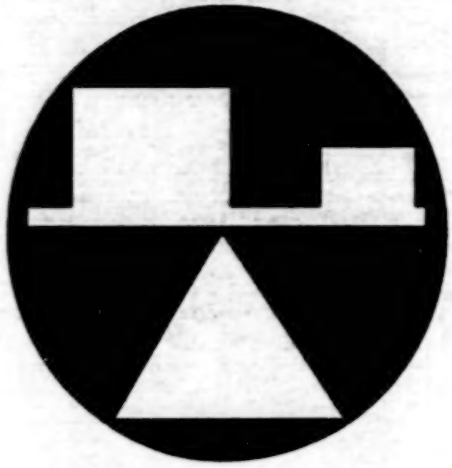

Mechanics

Hardware, Techniques, and Processes

35 Flex Wedges

36 Miniature Electroactive-Polymer Rakes

37 Heat-Shield Panels in a 2D Shingling Arrangement

38 Magnetically Actuated Miniature Paraboloidal Mirrors With Variable Radii of Curvature

BLANK PAGE

Flex Wedges

Brakes and clutches could perform more reliably and predictably.

Goddard Space Flight Center, Greenbelt, Maryland

Flex wedges have been proposed for use in brakes and clutches like those in which, heretofore, basic wedges have been used. Flex wedges (see Figure 1) offer advantages of superior braking and clutching performance and less weight, relative to basic wedges.

The upper part of the figure depicts part of a typical brake or clutch that contains a basic wedge that mates with the side walls of a groove in a fixture. To obtain braking or clutching action, one pushes the wedge into the groove to obtain friction between the wedge and the fixture. A large frictional force is obtained by utilizing the mechanical advantage afforded by the wedge/groove geometry to multiply the perpendicular-to-the-surface contact force between the wedge and the fixture.

The mechanical advantage, and thus the effectiveness of braking or clutching in the case of a basic wedge, is greater for wedge faces and groove walls that are more nearly parallel. Unfortunately when these contact surfaces are fabricated more nearly parallel, there is a greater tendency for a wedge to become jammed in a fixture once it has been pushed in; as a result, the force needed to remove the wedge from contact with the fixture is larger and less predictable, and there is an increasing tendency for unjamming action to jerk the brake or clutch mechanism.

The lower part of the figure depicts part of a typical brake or clutch similar to that of the upper part of the figure, except for the use of a flex wedge instead of a basic wedge. This mechanism functions similarly to the basic-wedge mechanism, except that it offers enhanced holding performance, reliability, and predictability. Less actuation force is needed for both insertion and removal of the wedge; even unjamming requires little force and hence gives rise to little or no jerk.

The flex wedge (see Figure 2) is regarded as having been fabricated by machining away most of the material from a basic wedge. The flex wedge includes wedge shoes connected, via shoe flexures, to a wedge compliance flexure. The wedge shoes mate with the side walls of the groove in the fixture, in the same manner as that of the basic wedge. The wedge compliance flexure is made flexible with respect to motion in the x direction to accommodating small motions needed to align the wedge shoes with the side walls of the groove in the fixture. However, the wedge compliance fixture is stiff along the axis of insertion and removal (the y axis) and along the axis of the relative motion (the z axis) that the brake or clutch was meant to resist when engaged.

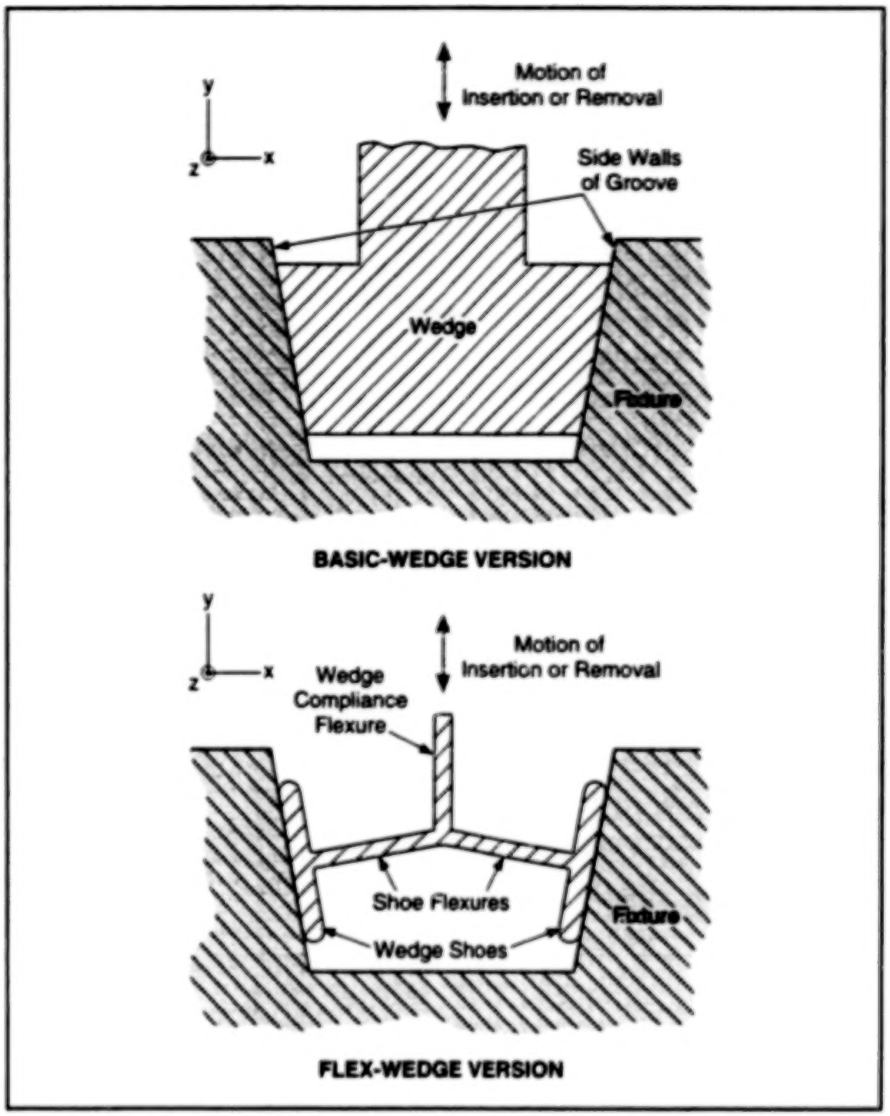

Figure 1. **These Parts of a Brake or Clutch** generate large contact forces between the wedge and groove surfaces in order to generate large friction forces to resist relative motion in the z direction. The flex wedge offers advantages over the basic wedge, as described in the text.

The shoe flexures are perpendicular to the wedge shoes, affording an additional mechanical advantage (beyond that of the basic wedge geometry) for both engagement and disengagement of the brake or clutch: Once the flex wedge was inserted as far as it could go, further pushing of the flex wedge into the fixture gives rise to a slight bend of the shoe flexures with consequent pushing of the wedge shoes into tighter contact with the side walls of the groove. Hence, the perpendicular-to-the-surface contact force (and thus the desired frictional braking or clutching force) for a given insertion force is greater than that for a basic wedge.

Even if the wedge shoes were pushed very tightly against the side walls, as described in the preceding paragraph, disengagement does not depend on the application of a large unjamming force. This is because pulling on the wedge compliance flexure in an effort to disengage the brake or clutch would first cause the shoe flexures to bend oppositely to the way they bent during insertion and this bend pulls

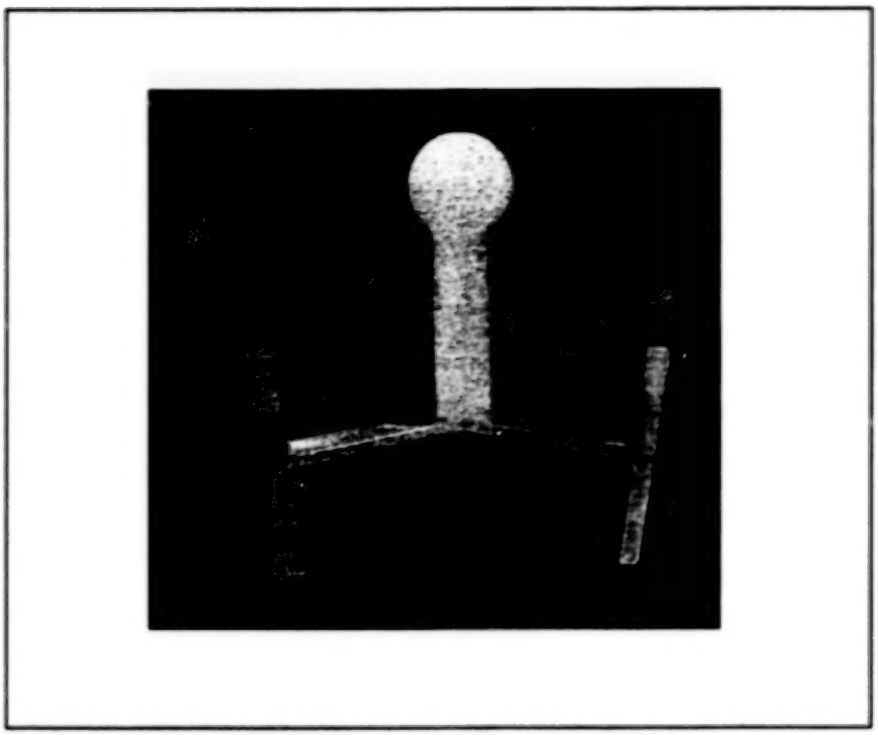

Figure 2. A photograph of the **Flex Wedge** shows the key components.

the shoes out of contact with the side walls of the groove. This disengagement action is characterized by a mechanical advantage that depends only on geometry (and not on the coefficient of friction). Hence, the force needed for extraction or disengagement would be small and predictable.

The shoe flexures are made thin and flexible to allow bending in the parallel-to-the-shoe directions, yet stiff as needed in the perpendicular-to-the-shoe directions. They are also made long in the z direction, as needed for strength and rigidity in holding against the relative motion that the brake or clutch is meant to resist when engaged.

This work was done by John M. Vranish of **Goddard Space Flight Center**. *Further information is contained in a TSP [see page 1].*

This invention is owned by NASA, and a patent application has been filed. Inquiries concerning nonexclusive or exclusive license for its commercial development should be addressed to the Patent Counsel, Goddard Space Flight Center [see page 1]. Refer to GSC-14006.

Miniature Electroactive-Polymer Rakes

Unwanted particulate matter in remote instrumentation settings would be removed by simple actuators.

NASA's Jet Propulsion Laboratory, Pasadena, California

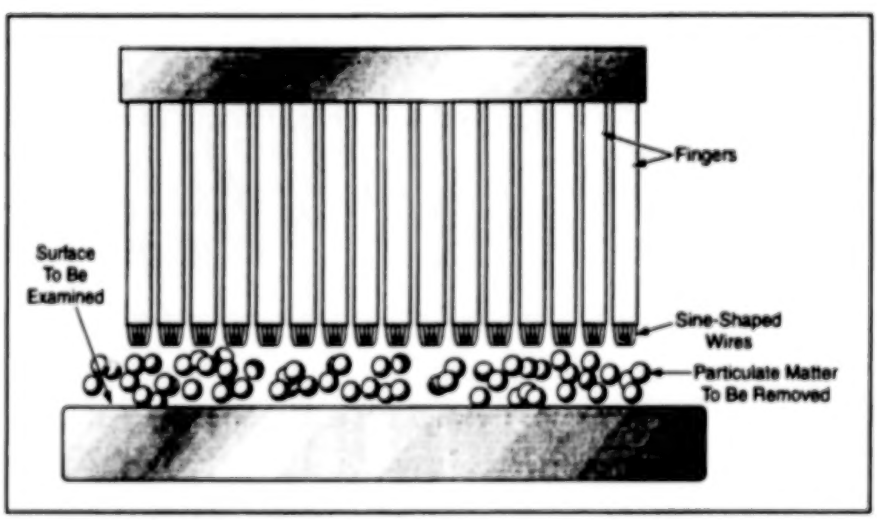

Figure 1. **A Miniature Electroactive Polymer Rake** contains actuator fingers that bend when voltage is applied. Overlapping sine-shaped wires on the tips enhance the raking action. Ground wires (not shown) at the tips prevent the accumulation of static electric charges.

Miniature electroactive-polymer rakes (MEARs) are undergoing development for eventual use as simple, lightweight, inexpensive low-power-consumption devices that would remove soil, dust, and/or other loose particulate matter from the surfaces of solid objects. In the original intended application, MEARs is being sought for use, in exploration of remote planets, to expose surfaces of rocks for examination by video cameras and/or other optoelectronic instruments. MEARs could also be used in similar remote-control geological exploration on Earth.

Unlike the tines in an ordinary rake, the tines in a MEAR are actuator fingers that bend under electrical control. Each finger consists mostly of a sandwichlike composite of (1) an inner layer comprising an ion-exchange-polymer membrane between (2) two outer polymeric layers that contain or are coated with gold or platinum and that serve as electrodes. The amount and direction of bending depends on the magnitude and polarity of the potential (typically of the order of several volts) applied between the electrodes. An alternating potential can be applied to obtain a repetitive raking or sweeping action. As described thus far, the MEAR fingers are nearly identical to the bending actuators described in "Robot Hands With Electroactive-Polymer Fingers" (NPO-20103), *NASA Tech Briefs*, Vol. 22, No. 10, (October 1998), page 78 and "Wipers Based on Electroactive Polymeric Actuators" (NPO-20371), *NASA Tech Briefs*, Vol. 23, No. 2 (February 1999), page 7b.

Figure 1 is a drawing of a typical MEAR. To enhance the raking action, wires made from aromatic polyamid fibers and bent into sine curves are attached to the tips of the actuator fingers. To prevent the potential accumulation of static electric charges from the rubbing of the fingers and/or sine-shaped wires on other objects, copper ground wires are added to the tips.

Figure 2 schematically depicts a variant of the basic MEAR concept for removing dust from a glass window. In this case, the window would be wiped by either a MEAR with metal-coated fingers or else by a metal-coated electroactive-polymer wiper like those described in the noted previous article about wipers. To remove charged particles and dust from the window, a large positive or negative dc potential difference would be applied between the window frame and the MEAR fingers or wiper. From time to time, the polarity of the applied dc potential would be switched.

This work was done by Yoseph Bar-Cohen and Sean Leary of Caltech for **NASA's Jet Propulsion Laboratory**. *Further information is contained in a TSP [see page 1].*
NPO-20613

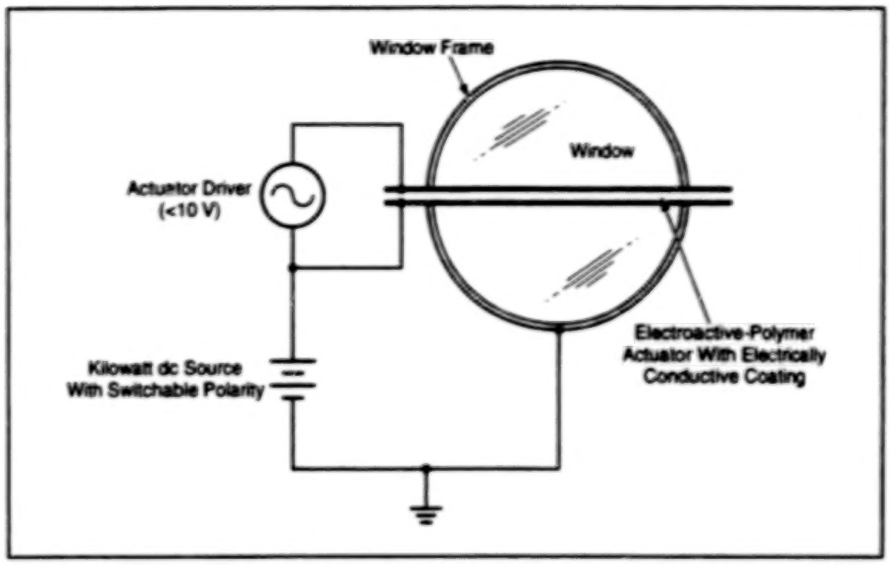

Figure 2. A Window Wiper containing one or more electroactive-polymer actuators and high-voltage circuitry would remove charged particles and dust.

Heat-Shield Panels in a 2D Shingling Arrangement

Adjacent panels are slid aside to make room for insertion or removal.

Marshall Space Flight Center, Alabama

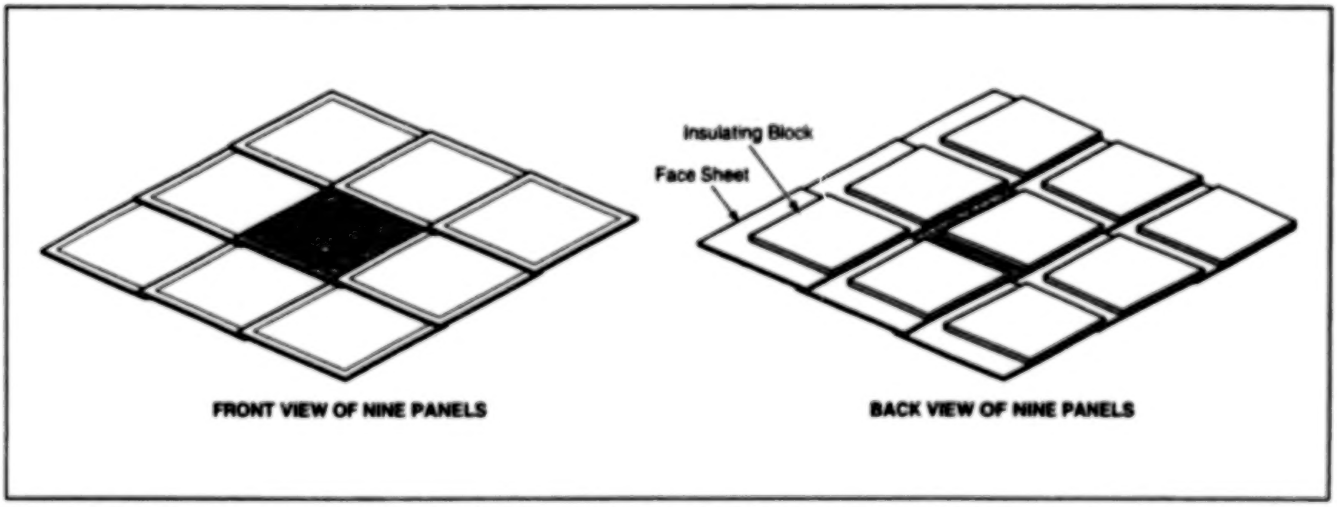

Figure 1. Panels Overlap and thus interlock in a two-dimensional shinglelike pattern. However, the interlock can be removed locally, to enable insertion or removal of a given panel, by simply sliding the overlapping parts of two adjacent panels out of the way.

Figure 1 depicts mockups of lightweight metal heat-shield panels that have been proposed for use on spacecraft of the reusable-launch-vehicle type. These panels are designed for simplicity of insertion and removal. The design could also be adapted to both insulating and noninsulating panels in nonspacecraft applications.

Each panel includes a thin front (outer) face sheet bonded to a thicker insulating block. The insulating block occupies an area slightly smaller than that of the face sheet and is located off center on the rear (inside) surface of the face sheet in such a way as to leave flange areas on two sides of the face sheet.

The panels are installed on stand-off brackets on a framework, as shown in Figure 2. When installation is complete, the two flanges of each panel overlap the non-flanged edge areas of two adjacent panels. In other words, the panels are overlapped in a two-dimensional (2D) generalization of the common shingling pattern.

The overlap creates an interlock that, in the case of a simple shingling arrangement, would make it necessary to remove many other panels in order to replace a given panel. However, unlike a simple shingling arrangement, this design provides for the removal of any given single panel without having to remove other panels; the panels, framework, and stand-off brackets are configured so that the panels can slide over each other in the front-surface plane. All one need do to remove the interlock from a given panel (e.g., the middle panel in Figure 1) is to push the overlapping adjacent panels to slide their flanges off the given panel.

This work was done by Dalton Nguyen of **Marshall Space Flight Center**. *Further information is contained in a TSP [see page 1].*
MFS-31266

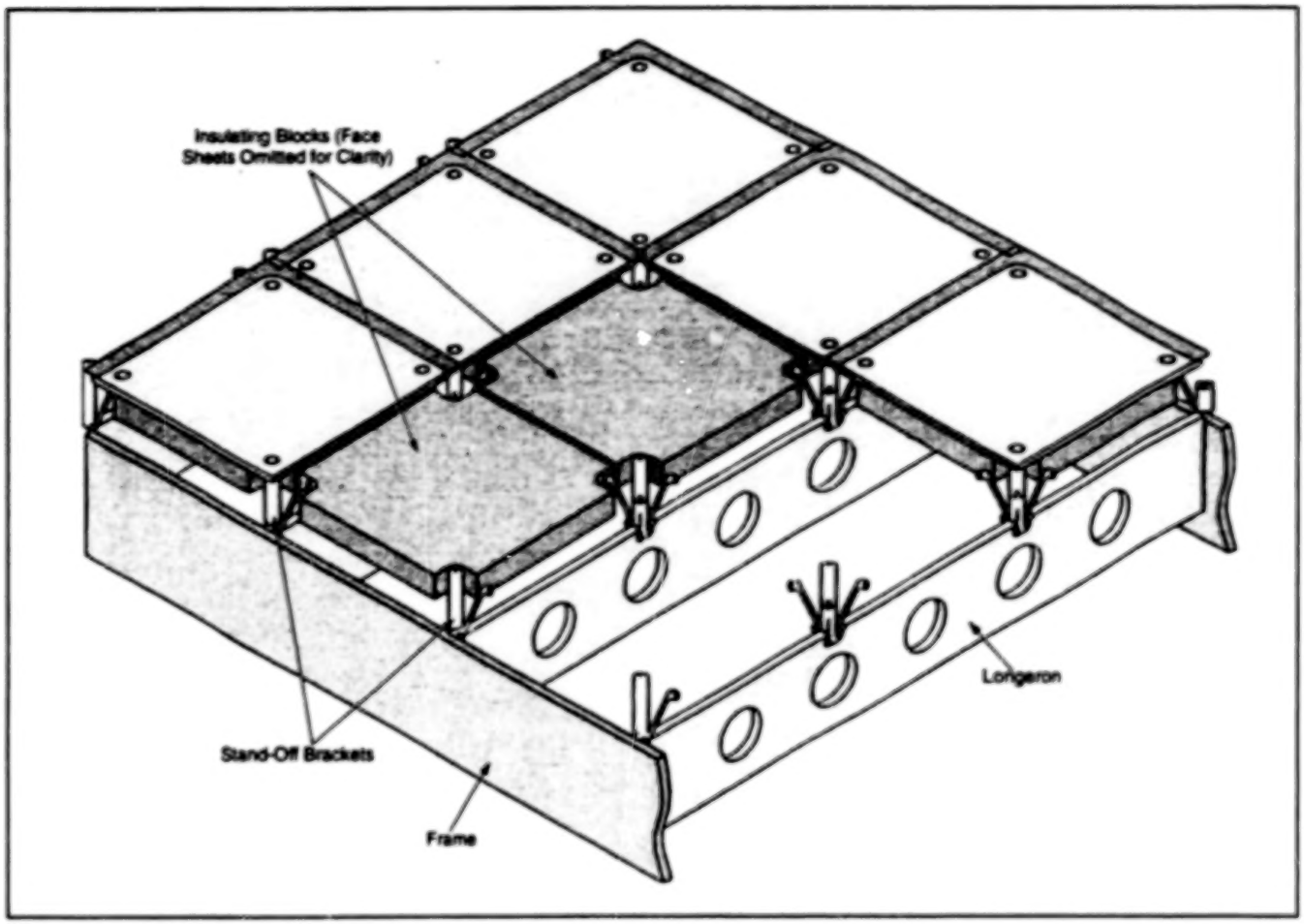

Figure 2. **Panels Are Supported** on a framework in such a way that they can be slid aside to insert or remove one panel without having to insert or remove others at the same time.

Magnetically Actuated Miniature Paraboloidal Mirrors With Variable Radii of Curvature

These are intended to supplant conventional components, reducing the bulkiness associated with focusing and zooming mechanisms.

NASA's Jet Propulsion Laboratory, Pasadena, California

Design and development of miniature paraboloidal mirrors that would be deflected magnetically to vary their radii of curvature (and thus their focal lengths) are under study. These mirrors, which belong to the class of microelectromechanical systems (MEMS) are used for compact, robust, focusing optics instruments and imaging systems, and are intended to supplant conventional adjustable optical components (including lenses, curved mirrors, and hinged flat mirrors) for reducing the bulkiness of the associated focusing and zooming mechanisms. The suggested device (see figure) would include a thin paraboloidal diaphragm mounted at a short axial distance from a planar coil; the concave side of the diaphragm would serve as the mirror, the convex side of the diaphragm would face the planar (concentric) coil

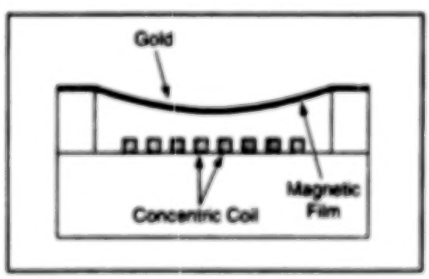

MEMS Magnetic Multifunctional Mirror system design illustrates the key components.

and would be coated with thin layer of magnetic material. Electron-beam binary-optics and low-pressure chemical vapor deposition (LPCVD) processes are used to form the paraboloidal concave surface, and the radio-frequency sputtering process is used to form the thin magnetic layer. At the same time, electroplating is used for the fabrication of the planar coil on silicon wafer. The two wafers would then be bonded together to form the mirror-and-actuator unit.

This approach to miniaturization offers several potential advantages in that the magnetic actuation forms the integral part of the optical sensing mechanism (including beam focusing and steering), thus reducing the overall size of the mirror. Also, the actuation sensitivity would be higher due to the high coefficient of elasticity of the magnetic layer, thus deflections attainable by the proposed approach would be higher than those attainable with electrostatic or piezoelectric actuations.

This work was done by Mary Boghosian and William Tang of Caltech for **NASA's Jet Propulsion Laboratory**. *Further information is contained in a TSP [see page 1].*

NPO-20949

Machinery

Hardware, Techniques, and Processes

41 Actuated Ball-and-Socket Joints
42 Ultrasonic Detector and Identifier of Land Mines
43 Subsurface-Explorer Robot With Spinning-Hammer Drive

Books and Reports

44 Modular Propulsion Clusters
44 Positioning System for a Human Habitat in a Large Centrifuge
44 Launch-on-Demand Servicing Microsatellites
45 Miniature Electrothermal Thruster

BLANK PAGE

Actuated Ball-and-Socket Joints

These joints would be relatively compact, lightweight, simple, and inexpensive.

NASA's Jet Propulsion Laboratory, Pasadena, California

The term "actuated ball-and-socket" (ABS) characterizes a proposed class of ball-and-socket joints that would incorporate ultrasonic motors and other piezoelectric actuators to generate multidimensional actuation. In some applications, ABS joints could supplant traditional joint-and-actuator assemblies that include passive rotary joints actuated by electromagnetic motors via gears. In comparison with such assemblies, ABS joints offer potential advantages of compactness, relative mechanical simplicity, higher torque-to-weight ratios, no backlash, self-braking with power turned off, and lower cost. ABS joints are expected to be particularly attractive for use as robot joints and as general low-power orienting actuators for diverse applications that could include robot hands, tools, and mechanisms for aiming scientific instruments.

Figure 1 illustrates an ultrasonic motor similar to those that would be included in an ABS joint. This motor includes a washerlike rotor spring-loaded into contact with a washerlike stator. The stator includes a ring of piezoceramic actuator elements that are bonded to a base stator substructure, on the stator face opposite that in contact with the rotor. The piezoceramic elements are positioned at circumferential intervals and are electrically connected in alternating polarity. When electrically excited by waveforms with a proper phase difference, the piezoceramic elements deform in such a manner as to induce a wave that travels circumferentially around the stator. This wave can be amplified by the resonance of the stator and can have an amplitude of the order of several micrometers. As this wave travels around the stator, it causes points on the free surface of the edge of the stator to travel in small elliptical orbits. At crests of the wave, the stator pushes against the rotor, so that through friction, some of the elliptical motion is converted to rotary motion of the rotor.

Figure 2 depicts an ABS joint. A spherical rotor would fit in a housing that would contain bearings. The housing would also contain three drive units (A, B, and C) — each for rotation about one of three axes. These axes, which span three-dimensional space, intersect at the center of the rotor. (The axes are not necessarily perpendicular.) Power and control cables would be connected to each drive unit.

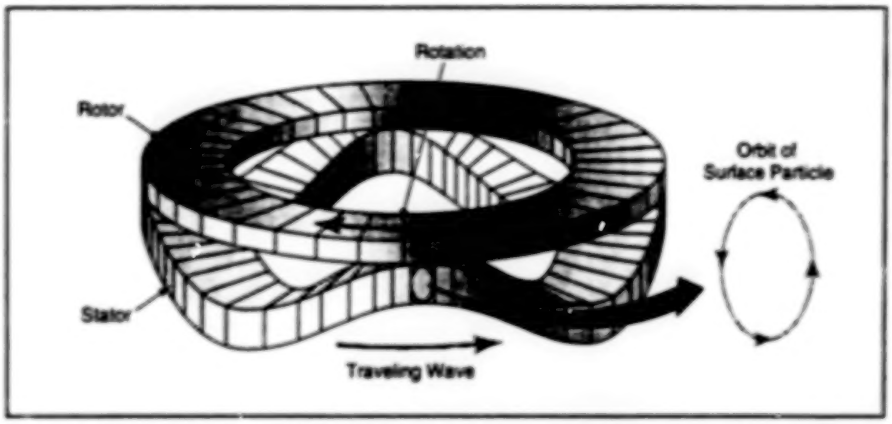

Figure 1. **Small Elliptical Orbital Motion** of a point on the surface of the stator under the influence of a traveling wave causes (through friction) the rotor to move in a circumferential direction opposite that of the propagation of the wave.

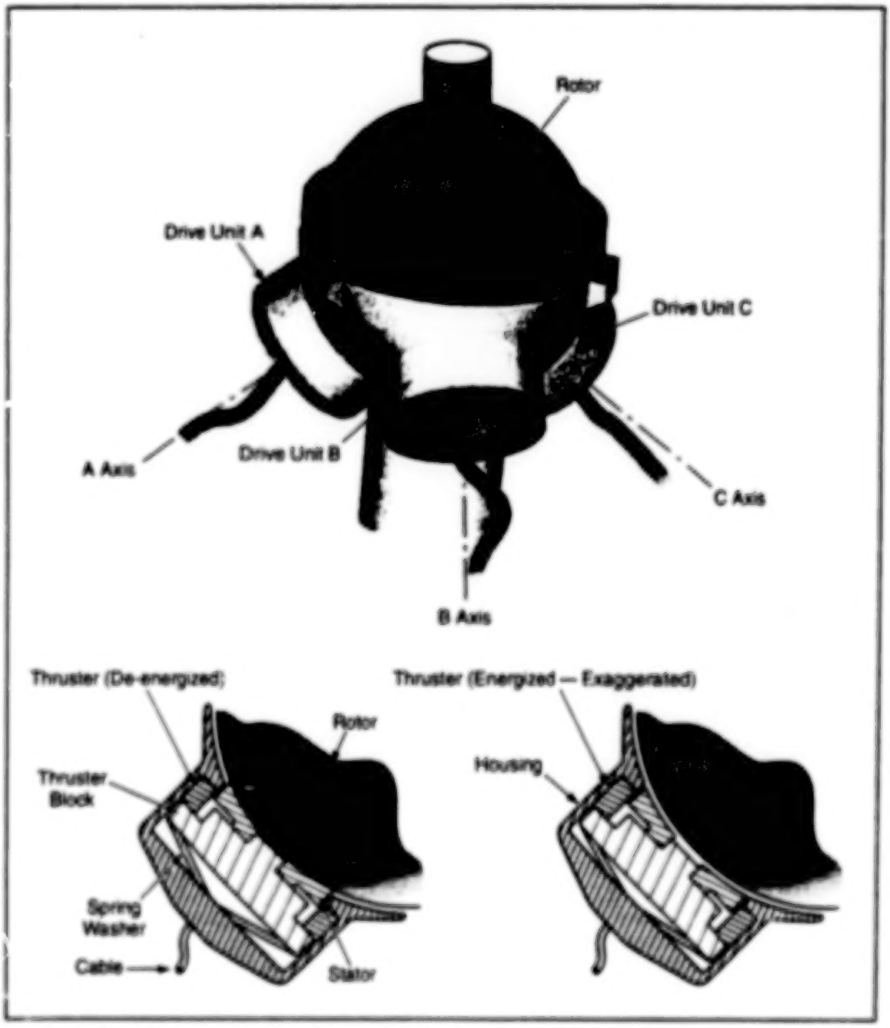

Figure 2. An **ABS Joint** would contain an ultrasonic motor plus a thruster that could disconnect the motor stator from the rotor.

Within each drive unit, a thruster block would support an ultrasonic-motor stator. This stator would likely be somewhat more complex than that of Figure 1: among other things, its rotor-contact surface

would likely be spherical, with a radius matching that of the rotor. Notwithstanding the added complexity, the basic principle of operation would be the same as that of the ultrasonic motor described above. By suitable electrical excitation of the stator, the rotor could be made to rotate about the axis of symmetry of the drive unit. A spring washer would push the thruster block, and thus the stator, radially against the rotor. The rotor/stator friction associated with this radial preload would establish the holding (braking) torque in the absence of applied power.

A piezoceramic ring, denoted the thruster, would be located between the thruster block and a shelf in the housing. When not energized, the thruster would not exert any effect. When electrically energized, the thruster would push the thruster block radially outward (against the spring washer), thereby pulling the stator out of contact with the rotor. Thus, energizing the thruster would prevent the drive unit from either driving or braking the rotor.

To avoid working against the holding torque of the other drive units, only one drive unit at a time could be used to produce rotation. For example, in order to obtain rotation about axis A, it would be necessary to (1) excite the stator of drive unit A with appropriately phased waveforms while (2) energizing the thrusters of drive units B and C to prevent these units from braking the rotation about axis A. To move the rotor from an initial orientation to a desired final orientation, it would be necessary to generate a trajectory consisting of a sequence of small rotations about the A, B, and C axes. It would be necessary to develop an electronic data-processing and control system to compute and implement the coordinated, sequential actuation of the three thrusters and the three ultrasonic-motor stators to generate the trajectory. It has been estimated that, in a typical application, the increments of rotation would be characterized by frequencies of the order of a kilohertz.

This work was done by Issa Nesnas of Caltech for **NASA's Jet Propulsion Laboratory**. *Further information is contained in a TSP [see page 1].*
NPO-20984

Ultrasonic Detector and Identifier of Land Mines

It would no longer be necessary to put human searchers at risk.

NASA's Jet Propulsion Laboratory, Pasadena, California

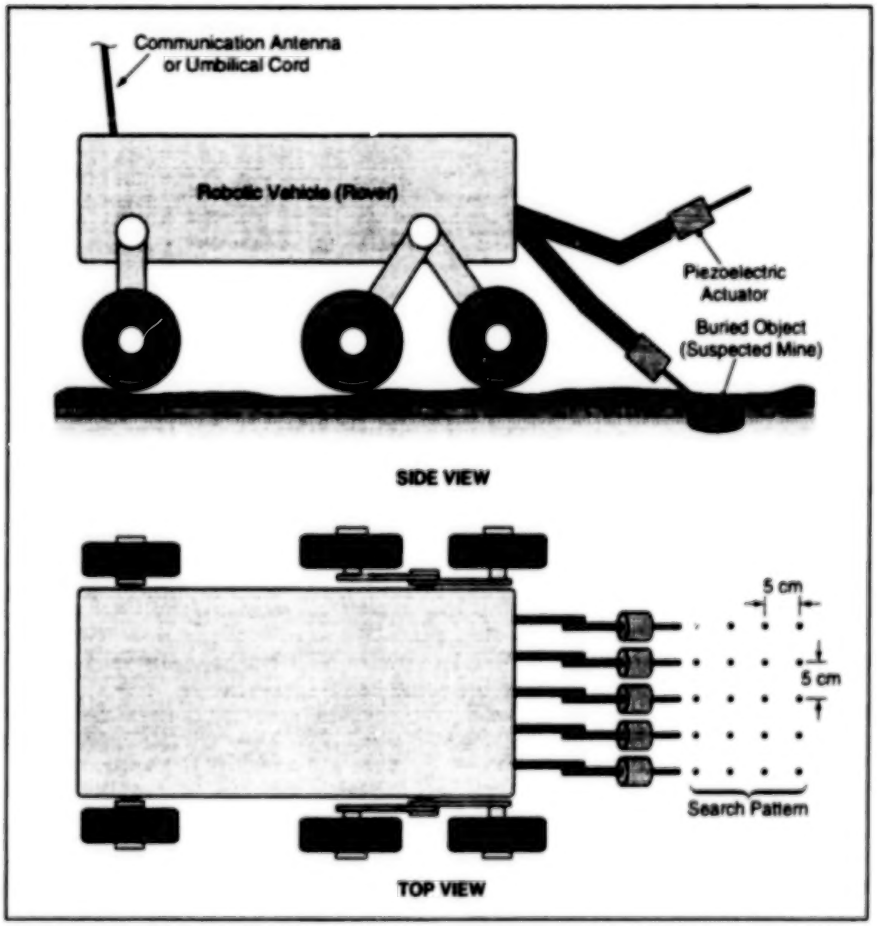

Ultrasonically Vibrating Prods would be inserted in the ground, in a manner similar to that of a manual search for mines. The robotic vehicle could also be equipped with an arm for digging up and removing mines.

A robotic apparatus equipped with ultrasonic probes and other instrumentation has been proposed to reduce the danger and cost and increase the speed of searching for land mines. The apparatus would implement modified versions of the proven techniques used by human searchers (delicately probing for, and excavating around, suspected objects) aided by dogs trained to sniff out explosives.

The instrumentation would be mounted on a robotic vehicle (see figure). The ultrasonic probes would include 30-cm-long prods that would be inserted gently in the ground at angle of about 30°, as in manual demining. Piezoelectric actuators at the upper ends of each probe would vibrate the prod at a frequency of about 20 kHz. The probes would be placed 5 cm apart in a comblike structure, and the vehicle would move in 5-cm steps. Thus, the search pattern would be a square array of points at intervals of 5 cm.

Although all the probes would be operated simultaneously, each would be pushed into the ground under separate control to search for hard objects. The insertion mechanism for each probe would be instrumented to measure the position, speed, and force of insertion. Contact between a probe tip and a buried mine, rock, or other hard object would be indicated by a sharp increase in the force and a corresponding sharp decrease in the speed of insertion. Once an object suspected of being a mine had been detected, probes could be inserted at various positions and angles to determine the size, shape, and location of the object. The force applied by the insertion mechanism would be limited to a level (preferably <10 N) below the force that could detonate a mine. The speed of insertion would also be limited to prevent accidental

impact and detonation.

The prods would be in the form of hollow tubes, through which dust kicked up by the vibrations could be collected and analyzed. In particular, the vibrating tip of a prod could scratch the surface of a suspected object and the resulting dust could be analyzed by use of a miniature onboard mass spectrometer to determine whether the surface is a plastic, metal, wood, or other material of a suspected mine case. The effect of a suspected object on the acoustic impedance of the ultrasonic transducer in each probe would be examined to obtain additional information about a suspected object. Other sensors and actuators could also be used; for example, an eddy-current sensor could be used to detect a metallic surface, and localized heat could be applied to melt or decompose a small amount of surface material for analysis. Information acquired through multiple sensors could be processed by a sensor-fusion algorithm in an effort to confirm that a suspected object is a mine and, if possible, identify the type of mine. The algorithm would incorporate expert-system and other artificial-intelligence software.

This work was done by Yoseph Bar-Cohen of Caltech for **NASA's Jet Propulsion Laboratory**. *Further information is contained in a TSP [see page 1].*
NPO-20399

Subsurface-Explorer Robot With Spinning-Hammer Drive

The robot would bury itself by internally generated hammer blows.

NASA's Jet Propulsion Laboratory, Pasadena, California

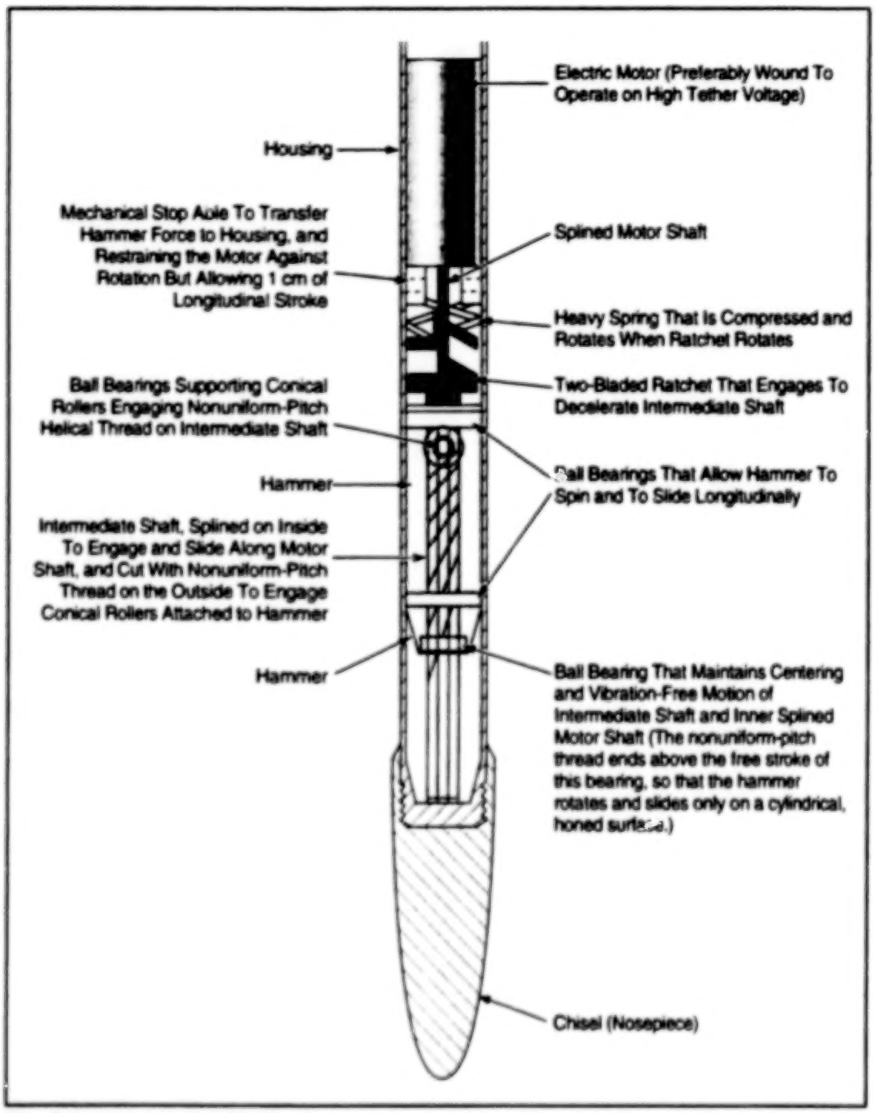
Electric Motor (Preferably Wound To Operate on High Tether Voltage)
Housing
Mechanical Stop Axle To Transfer Hammer Force to Housing, and Restraining the Motor Against Rotation But Allowing 1 cm of Longitudinal Stroke
Splined Motor Shaft
Heavy Spring That Is Compressed and Rotates When Ratchet Rotates
Two-Bladed Ratchet That Engages To Decelerate Intermediate Shaft
Ball Bearings Supporting Conical Rollers Engaging Nonuniform-Pitch Helical Thread on Intermediate Shaft
Ball Bearings That Allow Hammer To Spin and To Slide Longitudinally
Hammer
Intermediate Shaft, Splined on Inside To Engage and Slide Along Motor Shaft, and Cut With Nonuniform-Pitch Thread on the Outside To Engage Conical Rollers Attached to Hammer
Hammer
Ball Bearing That Maintains Centering and Vibration-Free Motion of Intermediate Shaft and Inner Splined Motor Shaft (The nonuniform-pitch thread ends above the free stroke of this bearing, so that the hammer rotates and slides only on a cylindrical, honed surface.)
Chisel (Nosepiece)

The Spinning-Hammer Mechanism in the subsurface-explorer robot would effect action similar to that of a jackhammer. However, unlike a jackhammer, the mechanism would be specially designed to maximize performance in operation of the robot in a self-burying mode and to obtain operating power from a high-voltage, low-current external source.

A proposed robotic apparatus for underground exploration would propel itself downward in a percussive manner reminiscent of a jackhammer, pile driver, or hammer-and-chisel combination. Called a "subsurface explorer" (SSX), the apparatus (see figure) would include a hammer that would be moved within a generally cylindrical housing to repeatedly strike a chisel in the form of a rounded nosepiece at its front (lower) end. Each impact of the hammer on the chisel would give rise to an impact of the chisel on the rock and/or soil at the front. The rock (if any) at the front end would be crushed into fine particles. Upon each impact, the apparatus would advance a small distance downward; concomitantly, the soil and/or rock particles would flow upward relative to the housing and would become recompacted behind (above) the apparatus. Thus, the apparatus would bury itself and, unlike in drilling, there would be no need to remove ground material to form a hole.

The apparatus could carry sensors, sensor circuitry, and control circuitry, all loosely sprung inside the housing for protection against shocks from hammer blows. Inertial sensors could measure stroke lengths for purposes of feedback control and estimating speed and depth of penetration. An array of geophones on the surface could measure echoes of the percussions for purposes of locating the apparatus and mapping the subsurface environment.

The vehicle would be driven electrically from a high-voltage, low-current power source above the surface. The power would be delivered via a pair of hair-thickness insulated wires that would be paid out from the rear (upper) end of the vehicle and would thus become buried in the overlying displaced material. According to preliminary design estimates based on a cross section and hammer impacts comparable to those of a manually driven sledge hammer about once every 10 seconds, a time-averaged delivered power of about 50 to 100 W would be needed to effect an advance of about 0.4 mm/s through typical rock. Digital signals for control and for sensor readouts could be superimposed on the relatively steady supply voltage.

A major innovative aspect of the apparatus would lie in electromechanical means for converting the trickle of supplied power into the periodic bursts of energy (about 500 J per burst) needed to effect the hammer blows. The hammer — essentially a massive hollow cylinder — would be mounted on bearings on an intermediate shaft that would be splined to turn with, and slide along, the shaft of an electric motor. In the first phase of an operating cycle, the motor would be used to spin the hammer around the longitudinal axis to store energy as in a flywheel.

Once the hammer was rotating at maximum speed, the motor would be braked. However, the hammer would continue to rotate. Conical rollers inside the rotating hammer would engage nonuniform helical threads on a shaft, causing the rotation of the hammer to be converted into longitudinal translation. The threads would be configured so that the hammer would undergo approximately constant longitudinal acceleration toward the chisel, and so that at the impact of the hammer upon the chisel, most of the rotational kinetic energy would have been converted to translational kinetic energy.

After impact, the motor would be spun up once again. By virtue of the engagement between the conical rollers and the nonuniform helical threads on the sides opposite those of the engagement for the downward stroke, the hammer would be made to translate back up to the starting position. The cycle described thus far would then be repeated.

This work was done by Brian H. Wilcox of Caltech for **NASA's Jet Propulsion Laboratory**. *Further information is contained in a TSP [see page 1].*

In accordance with Public Law 96-517, the contractor has elected to retain title to this invention. Inquiries concerning rights for its commercial use should be addressed to

Technology Reporting Office
JPL
Mail Stop 249-103
4800 Oak Grove Drive
Pasadena, CA 91109
(818) 354-2240

Refer to NPO-20614, volume and number of this NASA Tech Briefs *issue, and the page number.*

Books and Reports

Modular Propulsion Clusters

A report proposes the development of modular propulsion clusters (MPCs) — small, self-contained propulsion systems that would be standardized, mass-produced, and readily installed on a variety of miniature future spacecraft. The MPCs would be inexpensive, "turn-key" alternatives to expensive conventional propulsion systems that are designed and built integrally with other spacecraft systems and structures. Each MPC would contain its own propellant tank, isolation valve, gas plenum, and valve/nozzle thruster assemblies. Each MPC would be delivered fully loaded; installation on a spacecraft would involve only mounting and electrical connections. The propellant would be a liquid that, by electrical actuation of valves, would be metered into the plenum as needed to vaporize and generate thrust. An important advantage of using a vaporizing propellant liquid (as opposed to a propellant gas) is that stopping a liquid leak is orders of magnitude easier than is preventing a gas leak.

This work was done by Barry Nakazono of Caltech for **NASA's Jet Propulsion Laboratory**. *To obtain a copy of the report, "Modular Propulsion Cluster," see TSP's [page 1].*
NPO-20783

Positioning System for a Human Habitat in a Large Centrifuge

A report describes the system for controlling the radial position and tilt of a spacecraftlike habitat for humans in NASA's Space Flight Environmental Simulator (SFES) — a 16-m-diameter centrifuge used previously to evaluate effects of hypergravitational acceleration on animals. The habitat-positioning system was installed as an upgrade of the SFES to enable similar testing on humans to obtain guidance for designing centrifugal artificial-gravitation systems for future spacecraft. The radial position of the habitat is adjusted by a non-back-driveable acme-screw mechanism actuated manually via a crank. The tilt of the habitat is adjusted by an acme-screw slider-crank mechanism driven by a dc brushless motor in response to feedback control that strives to maintain zero effective acceleration/gravitation as measured by an accelerometer located in, and oriented parallel to the floor of, the habitat. The reason for doing this rather than simply mounting the habitat on gimbals so that it would actively align itself with the local gravitation/acceleration is that the feedback control is needed for stability: In the absence of such control, movement of occupants and equipment would cause undesired rocking of the habitat.

This work was done by W. F. Caldwell, Jr., of **Ames Research Center**, *J. Tucker of Gates/Arrow Distributing, and P. Keas of Sverdrup Technology, Inc. To obtain a copy of the report, "Human Habitat Positioning System for NASA's Space Flight Environmental Simulator," see TSP's [page 1].*
ARC-14331

Launch-on-Demand Servicing Microsatellites

A report describes an emerging class of miniature, highly capable, relatively inexpensive satellites that could be launched rapidly by nontraditional methods. Of particular interest is a subclass of proposed launch-on-demand microsatellites for inspecting and servicing other satellites (targets) already in orbit. A satellite of this subclass would have a mass of ≤ 30 kg and could be launched, by use of a modified missile system, from a fighter airplane in flight. Equipped with a solid rocket motor and an onboard guidance system, the newly launched microsatellite would insert itself in orbit. Once in orbit, the microsatellite would maneuver by use of cold-gas thrusters to approach the target. An inspecting microsatellite would acquire images of the target from all relevant directions and transmit the image data to a ground station, then would descend from orbit. A servicing microsatellite would dock with a servicing port on the target and then would perform the service, which could include attaching new hardware, replenishing a depleted supply of a fluid, and/or transferring data or software. The servicing microsatellite would remain permanently docked with the target.

This work was done by George Jaivin of Caltech for **NASA's Jet Propulsion Laboratory**. *To obtain a copy of the report, "Novel Missions for Next Generation Microsatellites: The Results of a Joint AFRL/JPL Study," see TSP's [page 1].*
NPO-20813

Miniature Electrothermal Thruster

A report proposes a miniature electrothermal spacecraft engine. The engine would include a chamber with an inside length of ≈1.5 cm and inside diameter of ≈0.25 cm, with a dielectric (ideally diamond) sidewall lining, a metal-coated expansion nozzle at one end, and a metal electrode at the other end. A propellant liquid (ammonia) would be vaporized into the cavity. To heat the NH_3 vapor and dissociate it to a nitrogen/hydrogen plasma, the cavity would be excited with an electromagnetic field at a cavity resonance frequency of about 25 GHz (also the frequency of a dielectric resonance of NH_3). The expansion of the plasma through the nozzle would generate thrust. The electric field would be of such a strength and configuration as to prevent contact between the plasma and the inner surface of the chamber. The plasma skin depth would be great enough that the plasma could absorb a large proportion of the electromagnetic energy. By use of refractory electrode and dielectric materials, pulsed operation, and, preferably, evaporative cooling of the chamber wall by the propellant liquid, it should be possible to achieve high plasma temperature and pressure and, thus, high thrust.

This work was done by Frank T. Hartley of Caltech for **NASA's Jet Propulsion Laboratory**. *To obtain a copy of the report, "Miniature Microthermal Thruster," see TSP's [page 1].*

NPO-20969

BLANK PAGE

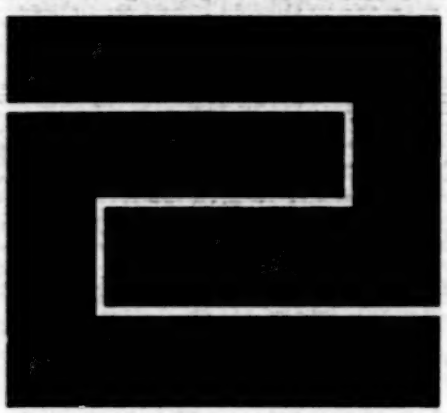

Fabrication Technology

Hardware, Techniques, and Processes

49 Study of Stitching Errors in Shot-Shifted E-Beam Lithography

BLANK PAGE

Study of Stitching Errors in Shot-Shifted E-Beam Lithography

A report presents a study of the efficacy of shot shifting for reducing stitching errors in diffraction gratings made by electron-beam (E-beam) lithography. Stitching errors arise from fabricating a grating as a mosaic of smaller gratings by frequently translating the grating blank. (This is done because typically, the required size of a grating exceeds that of the field swept by the electron beam.) In shot shifting, each field is written at a fraction of the total electron dose and the stage is moved the same fraction of a field width before writing the next field, so that the averaging effect of shifted multiple passes will suppress errors that arise from miscalibration between beam and translation-stage motions. In the study, a simplified linear model was used to describe the grating-writing process in the spatial-frequency domain. The origin and magnitude of stitching-error spatial-frequency sidebands was demonstrated. The effect of the multipass writing was shown to be equivalent to that of a band-pass filter that selectively nulls nearby sidebands. It was shown that *M*-order multipass writing suppresses only the nearest *M*–1 sidebands, and that increasing *M* results in restrictions on the allowable grating periods.

This work was done by David Dougherty, Paul Maker, and Richard Muller of Caltech for **NASA's Jet Propulsion Laboratory**. *To obtain a copy of the report, "Stitching Error Reductions in Gratings by Shot-Shifted Electron Beam Lithography," see TSP's [page].*
NPO-21072

BLANK PAGE

Mathematics and Information Sciences

Hardware, Techniques, and Processes

53 An Improved Genetic Algorithm for Optimal Spacecraft Scheduling
53 Timeout Algorithm for Communications With Long Delays
53 Software for Multidisciplinary Concurrent Optical Design

An Improved Genetic Algorithm for Optimal Spacecraft Scheduling

A genetic algorithm and heuristic routine are combined to improve scheduling performance.

NASA's Jet Propulsion Laboratory, Pasadena, California

A method of computing globally optimal schedules and plans in the face of possibly temporally varying constraints involves the use of an improved genetic algorithm. The method and computer program are directed toward the eventual use to schedule tasks to be performed on spacecraft.

The main problem in scheduling is to select the order and the starting and ending times of tasks so that they do not violate constraints; among other things, this means that the instantaneous aggregate demands of the tasks must not exceed the available resources (e.g., finite power-generating capacities) and that the tasks must be completed within the allowable time. One can treat a scheduling problem as a global-optimization problem if one embeds resource limits and other constraints into a cost or fitness function. One can then use a genetic algorithm to search the space of potential solutions.

The present genetic algorithm incorporates several improvements over a prior algorithm that result in better performance, including higher speed and improved schedules. One improvement is a heuristic routine (see figure) that takes the order of tasks as input and generates the starting times of the tasks as output.

```
input = order of tasks
output = starting times of the tasks

for time = first to last
   for task = first to last
      if task satisfies ordering constraints
         if task satisfies resource constraints
            starting time of the task = time;
         end
      end
   end
end
```

This Heuristic Routine generates feasible solutions for the improved genetic algorithm. This routine has been found to be particularly effective for scheduling tasks subject to resource and time constraints.

Another improvement is a capability for systematic incorporation of time and task ordering constraints. Specific tasks can now be forced to be performed before, after, or during other tasks, and/or specified absolute times. Time-out and nonoverlap constraints can also be applied. These new time and task ordering constraints are added to the resource constraints that were included in the prior algorithm.

Still another improvement is a capability for adaptive resequencing. In this mode, the genetic algorithm functions in an environment where resource constraints, time constraints, and task priorities can change at any time. Examples have shown that the algorithm works well, even when such changes are made during computation.

This work was done by David Bayard, Hamid Kohen, George Papavassilopoulos, and Il-Jun Jeong of Caltech for **NASA's Jet Propulsion Laboratory**. *Further information is contained in a TSP [see page 1].*
NPO-20884

Timeout Algorithm for Communications With Long Delays

Communications over long or intermittent links would be more efficient.

NASA's Jet Propulsion Laboratory, Pasadena, California

A query timeout detection algorithm has been proposed to support a protocol for reliable communications over links that are characterized by long delays because of (1) propagation of signals over interplanetary distances and/or (2) intermittency. The protocol could be an interplanetary analogue of Transmission Control Protocol/Internet Protocol (TCP/IP) of the terrestrial Internet. The protocol would enable the interconnection of the terrestrial Internet with the internets planned for Mars and other destinations in the Solar system. Potential beneficiaries include operators of space-exploration missions in the short term and commercial internet users in the long term.

"Timeout" as used here refers to a deadline for determining whether it is necessary to retransmit a packet of data because either the packet or an acknowledgement of the packet was not delivered. Timeout intervals can be estimated from signal-propagation times. However, in the presence of extremely long and variable propagation delays and/or intermittency of communication links, the proposed algorithm would estimate timeout intervals more accurately and thus make it possible to utilize available transmission time more efficiently.

In the proposed algorithm, a timeout interval would be represented as a sum of eight subintervals. Values of some of the subintervals would be estimated initially and used to determine a reasonable future time when their final values must be calculated. At that time, the sum of subintervals would be recalculated to determine a final deadline.

This work was done by Scott C. Burleigh of Caltech for **NASA's Jet Propulsion Laboratory**. *Further information is contained in a TSP [see page 1].*
NPO-20519

Software for Multidisciplinary Concurrent Optical Design

An optical designer can collaborate with other experts at different locations.

Marshall Space Flight Center, Alabama

The Integrated Optical Design Analyzer (IODA) is a computer program that facilitates multidisciplinary concurrent engineering of highly precise optical instruments. (IODA should not be confused with a multidisciplinary optical-system-analysis program, called "IMOS," that has been reported previously in *NASA Tech Briefs*.) IODA facilitates the exchange of data among analysts, designers, and other experts in different disciplines (e.g., optics, structural analysis, heat transfer, and electronics) needed for accurate design. IODA integrates the modeling efforts of a team of such experts and provides simplified means

for performing design trade studies.

IODA enables an optical designer to utilize advanced technical models, developed by experts in engineering disciplines other than optics, to optimize the design of an optical instrument. The optical designer need not be familiar with the details of the models. IODA is compatible with the Internet and can therefore enable the optical designer to integrate design inputs from other experts on the design team performing analyses on different computers at different locations.

In a sense, IODA can bring the various models developed by other experts to the optical designer's home computer system for use in the design process. IODA provides the optical designer with a user-friendly graphical user interface that enables this designer to easily gain access to the various models developed by other experts and manipulate selected model characteristics that influence the performance of the optical instrument to be designed. IODA then submits each model thus modified to its native computer system, receives the results of the computation on the modified model, and integrates the results with the detailed optical model for evaluation of the performance of the instrument.

This work was done by James D. Moore, Jr., and Charles P. DePlachett of SRS Technologies for **Marshall Space Flight Center**. *Further information is contained in a TSP [see page 1] or contact SRS Technologies at (256) 971-7000.*

Inquiries concerning rights for the commercial use of this invention should be addressed to the Patent Counsel, Marshall Space Flight Center [see page 1]. Refer to MFS-31452.

Life Sciences

Books and Reports

57 Using Photosynthetic Bacteria To Make Oxygen on Mars

BLANK PAGE

Using Photosynthetic Bacteria To Make Oxygen on Mars

A report presents a proposal to harness photosynthetic bacteria to generate essential materials needed during human and robotic exploration on the surface of Mars. Utilizing an extremely small amount of H_2O and an ample amount of CO_2 (and N_2 and/or other elements and compounds) already present in the Martian environment, along with sunlight as the source of energy, the bacteria would produce O_2 and carbon-containing compounds (and nitrogen-containing compounds). The O_2 could be used to support human respiration and to burn fuels; the other compounds could be used, variously, to produce food and fuel or to grow green plants other than bacteria to produce food and fuel. The proposal would exploit the inherent capability of bacteria to reproduce and to adapt to changing environmental conditions. Bacteria to implement the proposal would be bred selectively and/or be genetically engineered for the intended applications, starting from candidate strains of natural terrestrial purple and green bacteria and cyanobacteria that can withstand harsh environments.

This work was done by Hamid Kohen of Caltech for **NASA's Jet Propulsion Laboratory**. *To obtain a copy of the report, "A Biologically Evolved and Genetically Engineered Bacteria for Facilitating Oxygen Delivery Throughout the Mars Advanced Outpost," see TSP's [page 1].*
NPO-20927

END

12-4-01